

# Lippmann-Schwinger Resonating-Group Formalism for $NN$ and $YN$ Interactions in an $SU_6$ Quark Model

Yoshikazu FUJIWARA, Michio KOHNO\*, Tadashi FUJITA, Choki NAKAMOTO\*\* and Yasuyuki SUZUKI\*\*\*

*Department of Physics, Kyoto University, Kyoto 606-8502*

*\*Physics Division, Kyushu Dental College, Kitakyushu 803-8580, Japan*

*\*\*Suzuka National College of Technology, Suzuka 510-0294, Japan*

*\*\*\*Department of Physics, Niigata University, Niigata 950-2181, Japan*

(Received September 4, 2021)

We formulate a Lippmann-Schwinger-type resonating-group equation to calculate invariant amplitudes of the quark-model baryon-baryon interaction. When applied to our recent  $SU_6$  quark model for the nucleon-nucleon and hyperon-nucleon interactions, this technique yields very accurate phase-shift parameters for all partial waves up to the energies of several GeV. The technique also has a merit of a straightforward extension to the  $G$ -matrix equation. A new analytic method is proposed to calculate the quark-exchange Born kernel for the momentum-dependent two-body interaction. The partial-wave decomposition in the momentum representation is carried out numerically. The invariant amplitudes are then used to calculate single-nucleon potentials in normal nuclear matter for high incident momenta  $q_1 \geq 3 \text{ fm}^{-1}$ , in which the so-called  $t^{eff}\rho$  prescription is found to be a good approximation to the single-particle potentials directly calculated in the lowest-order Brueckner theory.

## §1. Introduction

Though the quantum chromodynamics (QCD) is believed to be the fundamental theory of the strong interaction, it is still too difficult to apply it directly to two-baryon systems. At this stage a number of effective models have been proposed to understand the nucleon-nucleon ( $NN$ ) and hyperon-nucleon ( $YN$ ) interactions from basic elements of quarks and gluons.<sup>1)</sup> Among them the non-relativistic quark model has a unique feature that it enables us to take full account of a dynamical motion of the two composite baryons within a framework of the resonating-group method (RGM).<sup>2)</sup> The model describes confinement with a phenomenological potential and uses quark-quark ( $qq$ ) residual interactions consisting of a color analogue of the Fermi-Breit (FB) interaction. In the last several years, it was found that a proper incorporation of the meson-exchange effect is essential to make such a model realistic for the description of the  $NN$  and  $YN$  interactions.<sup>3), 4), 5), 6), 7), 8), 9), 10)</sup>

We have recently achieved a simultaneous description of the  $NN$  and  $YN$  interactions in the RGM formulation of the spin-flavor  $SU_6$  quark model.<sup>3), 4), 5), 6), 7)</sup> In this model the meson-exchange effect of scalar (S) and pseudo-scalar (PS) meson nonets is incorporated in the quark Hamiltonian in the form of effective meson-exchange potentials (EMEP) acting between quarks. The flavor symmetry breaking for the  $YN$  system is explicitly introduced through the quark-mass dependence of the Hamiltonian, as well as the flavor dependence of the exchanged meson masses.

An advantage of introducing the EMEP at the quark level lies in the stringent relationship of the flavor dependence, which is revealed in the various pieces of the  $NN$  and  $YN$  interactions. In this way we can utilize our rich knowledge of the  $NN$  interaction to minimize the ambiguity of model parameters, which originates from the scarcity of the present experimental data for the  $YN$  interaction.

We already have three different versions called RGM-F<sup>3),4)</sup>, FSS<sup>5),6),7)</sup> and RGM-H<sup>6),7)</sup>, differing in the treatment of the EMEP. The model called RGM-F introduces, besides the central force of the S-meson nonet, only the tensor component generated from the  $\pi$ - and  $K$ -meson exchanges, and uses some approximations in evaluating the spin-flavor factors of the quark-exchange RGM kernel. On the other hand, FSS and RGM-H calculate the spin-flavor factors explicitly at the quark level, and include the spin-spin terms originating from all members of the PS-meson nonet. The  $SU_3$  relation of the coupling constants emerges as a natural consequence of the  $SU_6$  quark model. For S-mesons, the  $F/(F+D)$  ratio turns out to take the  $SU_6$  value of purely electric type. This is too restrictive to reproduce existing experimental data for the low-energy  $YN$  cross sections. We relax this restriction in two ways; one is to change the mixing angle of the flavor-singlet and octet scalar mesons only for the  $\Sigma N(I = 3/2)$  channel, and the other is to employ the same approximation as RGM-F solely for the isoscalar S-mesons,  $\epsilon$  and  $S^*$ . We call these models FSS and RGM-H, respectively. Predictions of these two models are not very different except for the roles of the  $LS^{(-)}$  force in the  $AN - \Sigma N(I = 1/2)$  coupled-channel system. The  $SU_3$  parameters of EMEP, S-meson masses, and the quark-model parameters are determined to fit the  $NN$   $S$ -wave and  $P$ -wave phase shifts under the constraint that the deuteron binding energy and the  $^1S_0$  scattering length are properly reproduced. The low-energy cross section data for  $YN$  scattering are also employed to fix the parameters in the strangeness sector, especially the up-down to strange quark-mass ratio  $\lambda = m_s/m_{ud}$ . The reader is referred to the original papers<sup>6),7)</sup> for a full account of the models and the model parameters.

So far we have solved the coupled-channel (CC) RGM equation in the improved variational method developed by Kamimura<sup>11)</sup>. In this method each Gaussian basis function is smoothly connected to the positive- or negative-energy asymptotic waves, which are obtained by numerically solving a “local” CC Schrödinger equation consisting of the long-range one-pion tensor force and the other EMEP. Although this technique gives accurate results at laboratory energies up to about 300 MeV, it seems almost inaccessible to higher energies due to the rapid oscillation of the relative wave functions. In this paper we formulate an alternative method to solve the CC RGM equation in the momentum representation; namely, we derive a Lippmann-Schwinger-type RGM equation which we call an LS-RGM equation.\*) In this method all the necessary Born amplitudes (or the Born kernel) for the quark-exchange kernel are analytically derived by using a new transformation formula, which is specifically developed for momentum-dependent two-body interactions acting between quarks. The partial wave decomposition of the Born kernel is carried out numerically in the

---

\*) The idea to solve the RGM equation in the momentum representation, in order to avoid the rapid oscillation of relative wave functions at higher energies, is not new. See, for example, Ref. 12).

Gauss-Legendre integral quadrature. The LS-RGM equation is then solved by using the techniques developed by Noyes<sup>13)</sup> and Kowalski<sup>14)</sup>. Although this method requires more CPU time than the variational method, it gives very stable and accurate results over a wide energy range. Since we first calculate the Born amplitudes of the RGM kernel, it is almost straightforward to proceed to the  $G$ -matrix calculation.<sup>15)</sup>

As an application of the present formalism, we discuss single-particle (s.p.) potentials in normal nuclear matter. This application is motivated by the  $G$ -matrix calculation of the  $NN$  and  $YN$  interactions in the continuous prescription of intermediate spectra<sup>15)</sup>. The s.p. potentials of the nucleon and hyperons predicted by the model FSS have a flaw that they are too attractive in the momentum region  $q_1 = 5 \sim 20 \text{ fm}^{-1}$ . We will show that this particular feature of FSS is related to the ill-behavior of the spin-independent central invariant amplitude at the forward angles, which is traced back to too simple S-meson exchange EMEP in this model. We analyze this problem by using an approximation of the s.p. potential in the asymptotic momentum region, in terms of the  $T$ -matrix solution of the LS-RGM equation. This technique is sometimes called the  $t^{eff}_\rho$  prescription. We find that this procedure gives a fairly good approximation of the s.p. potentials predicted by the  $G$ -matrix calculation, even for such a small momentum as  $q_1 \sim 3 \text{ fm}^{-1}$  ( $T_{lab} \sim 200 \text{ MeV}$ ), as long as the real part of the s.p. potential is concerned.

In the next section we start from the standard RGM equation for the  $(3q)$ - $(3q)$  system and derive the LS-RGM equation in the momentum space. Appendix A gives a convenient formula to calculate the Born kernel of the quark-exchange RGM kernel. The formula is especially useful in the case of the momentum-dependent  $qq$  force. The Born kernel of FSS is explicitly given in §2.2 and in Appendix B. Since the flavor dependence of the spin-flavor factors plays an essential role in the application of the present formalism to the  $NN$  and  $YN$  interactions, the structure of the Born kernel and the scattering amplitudes is carefully described in §2.3 in terms of the Pauli-spinor invariants. Some useful expressions of the partial wave decomposition of the Born kernel and the invariant amplitudes are given in Appendices C and D, respectively. The  $t^{eff}_\rho$  prescription is derived in §2.4 as a method to calculate the asymptotic behavior of the s.p. potentials in the  $G$ -matrix calculation. In §3 we compare the phase-shift parameters obtained by the LS-RGM formalism with those by the improved variational method. The system we choose as an example is the most complicated system of the  $\Lambda N - \Sigma N (I = 1/2)$  channel coupling. The invariant amplitudes and the scattering observables of the  $NN$  system in the intermediate energies between  $T_{lab} = 400 \sim 800 \text{ MeV}$  are discussed in §4. The s.p. potential of the nucleon in normal nuclear matter is calculated in §5, by using the  $t^{eff}_\rho$  prescription. It is shown that the behavior of the spin-independent central invariant amplitude at the forward angles is related to the attractive behavior of the s.p. potentials around  $q_1 = 5 \sim 20 \text{ fm}^{-1}$  region. Also shown is a preliminary result of s.p. potentials in an improved model, which incorporates momentum-dependent higher-order terms of the S and vector (V) meson EMEP. Finally, §6 is devoted to a brief summary.

## §2. Formulation

### 2.1. *LS-RGM equation*

As mentioned in the Introduction, FSS<sup>5),6),7)</sup>, RGM-H<sup>6),7)</sup> and their preceding version RGM-F<sup>3),4)</sup> are formulated in the (3 $q$ )-(3 $q$ ) RGM applied to the system of two (0 $s$ )<sup>3</sup> clusters. The  $qq$  interaction is composed of the full FB interaction with explicit quark-mass dependence, a simple confinement potential of quadratic power law and EMEP acting between quarks. The RGM equation for the parity-projected relative wave function  $\chi_\alpha^\pi(\mathbf{R})$  is derived from the variational principle  $\langle \delta\Psi | E - H | \Psi \rangle = 0$ , and it reads as<sup>6)</sup>

$$\left[ \varepsilon_\alpha + \frac{\hbar^2}{2\mu_\alpha} \left( \frac{\partial}{\partial \mathbf{R}} \right)^2 \right] \chi_\alpha^\pi(\mathbf{R}) = \sum_{\alpha'} \int d\mathbf{R}' G_{\alpha\alpha'}(\mathbf{R}, \mathbf{R}'; E) \chi_{\alpha'}^\pi(\mathbf{R}') \quad , \quad (2.1)$$

where  $G_{\alpha\alpha'}(\mathbf{R}, \mathbf{R}'; E)$  is composed of various pieces of the interaction kernels as well as the direct potentials of EMEP:

$$\begin{aligned} G_{\alpha\alpha'}(\mathbf{R}, \mathbf{R}'; E) = & \delta(\mathbf{R} - \mathbf{R}') \left[ \sum_{\beta} V_{\alpha\alpha'D}^{(CN)\beta}(\mathbf{R}) + \sum_{\beta} V_{\alpha\alpha'D}^{(SN)\beta}(\mathbf{R}) \right. \\ & \left. + \sum_{\beta} V_{\alpha\alpha'D}^{(TN)\beta}(\mathbf{R}) (S_{12})_{\alpha\alpha'} \right] + \sum_{\Omega} \mathcal{M}_{\alpha\alpha'}^{(\Omega)}(\mathbf{R}, \mathbf{R}') - \varepsilon_\alpha \mathcal{M}_{\alpha\alpha'}^N(\mathbf{R}, \mathbf{R}') \quad . \quad (2.2) \end{aligned}$$

The subscript  $\alpha$  stands for a set of quantum numbers of the channel wave function;  $\alpha = [1/2(11) a_1, 1/2(11) a_2] SS_z Y I I_z; \mathcal{P}$ , where  $1/2(11)a$  is the spin and  $SU_3$  quantum number in the Elliott notation  $(\lambda\mu)$ ,  $a(= YI)$  is the flavor label of the octet baryons ( $N = 1(1/2)$ ,  $\Lambda = 00$ ,  $\Sigma = 01$  and  $\Xi = -1(1/2)$ ), and  $\mathcal{P}$  is the flavor-exchange phase.<sup>3)</sup> In the  $NN$  system with  $a_1 a_2 = NN$ ,  $\mathcal{P}$  becomes redundant since it is uniquely determined by the isospin as  $\mathcal{P} = (-1)^{1-I}$ . The relative energy  $\varepsilon_\alpha$  in the channel  $\alpha$  is related to the total energy  $E$  of the system through  $\varepsilon_\alpha = E - E_\alpha^{int}$  with  $E_\alpha^{int} = E_{a_1}^{int} + E_{a_2}^{int}$ . In Eq. (2.2) the summation over  $\Omega$  for the exchange kernel  $\mathcal{M}_{\alpha\alpha'}^{(\Omega)}$  involves not only the exchange kinetic-energy ( $K$ ) term, but also various pieces of the FB interaction, as well as several components of EMEP. The FB interaction involves the color-Coulombic ( $CC$ ) piece, the momentum-dependent Breit retardation ( $MC$ ) piece, the color-magnetic ( $GC$ ) piece, the symmetric  $LS$  ( $sLS$ ) piece, the antisymmetric  $LS$  ( $aLS$ ) piece, and the tensor ( $T$ ) piece, The EMEP contains the central ( $CN$ ) component from the S-mesons, and the spin-spin ( $SN$ ) and tensor ( $TN$ ) terms originating from the PS mesons. The contribution from a particular meson exchange is denoted by  $\beta$  in Eq. (2.2) only for the direct part of  $G_{\alpha\alpha'}(\mathbf{R}, \mathbf{R}'; E)$ . The explicit form of these  $qq$  forces is given in Refs. 6) and 16), and the corresponding basic Born kernel defined through

$$\begin{aligned} M_{\alpha\alpha'}^B(\mathbf{q}_f, \mathbf{q}_i; E) = & \langle e^{i\mathbf{q}_f \cdot \mathbf{R}} | G_{\alpha\alpha'}(\mathbf{R}, \mathbf{R}'; E) | e^{i\mathbf{q}_i \cdot \mathbf{R}'} \rangle \\ = & \langle e^{i\mathbf{q}_f \cdot \mathbf{R}} \eta_\alpha^{SF} | G(\mathbf{R}, \mathbf{R}'; E) | e^{i\mathbf{q}_i \cdot \mathbf{R}'} \eta_{\alpha'}^{SF} \rangle \quad (2.3) \end{aligned}$$

is given in the next subsection and Appendix B. Here  $\eta_\alpha^{SF}$  is the spin-flavor wave function at the baryon level, which is defined in Eq. (2.9) of Ref. 17).

To start with, we use the well-known Green function to convert the RGM equation Eq. (2.1) to an integral equation which has a parity-projected incident plane wave in the  $\alpha$  channel:

$$\begin{aligned} \chi_{\gamma\alpha}^\pi(\mathbf{R}, \mathbf{k}_\alpha) &= \delta_{\gamma,\alpha} \left[ e^{i\mathbf{k}_\alpha \cdot \mathbf{R}} + (-1)^{S_\alpha} \mathcal{P}_\alpha e^{-i\mathbf{k}_\alpha \cdot \mathbf{R}} \right] \\ &- \frac{1}{4\pi} \frac{2\mu_\gamma}{\hbar^2} \int d\mathbf{R}' \frac{e^{ik_\gamma |\mathbf{R}-\mathbf{R}'|}}{|\mathbf{R}-\mathbf{R}'|} \sum_\beta \int d\mathbf{R}'' G_{\gamma\beta}(\mathbf{R}', \mathbf{R}''; E) \chi_{\beta\alpha}^\pi(\mathbf{R}'', \mathbf{k}_\alpha) . \end{aligned} \quad (2.4)$$

Here  $\pi = (-1)^{S_\alpha} \mathcal{P}_\alpha = (-1)^{S_\beta} \mathcal{P}_\beta = (-1)^{S_\gamma} \mathcal{P}_\gamma$ , because of the parity conservation. The asymptotic wave of Eq. (2.4) with  $R \rightarrow \infty$  is given by

$$\begin{aligned} \chi_{\gamma\alpha}^\pi(\mathbf{R}, \mathbf{k}_\alpha) &\sim \delta_{\gamma,\alpha} \left[ e^{i\mathbf{k}_\alpha \cdot \mathbf{R}} + (-1)^{S_\alpha} \mathcal{P}_\alpha e^{-i\mathbf{k}_\alpha \cdot \mathbf{R}} \right] \\ &+ \frac{1}{k_\alpha} \sqrt{\frac{v_\alpha}{v_\gamma}} \frac{e^{ik_\gamma R}}{R} \left[ M_{\gamma\alpha}(\mathbf{k}_\gamma, \mathbf{k}_\alpha; E) + (-1)^{S_\alpha} \mathcal{P}_\alpha M_{\gamma\alpha}(\mathbf{k}_\gamma, -\mathbf{k}_\alpha; E) \right] , \end{aligned} \quad (2.5)$$

with  $\mathbf{k}_\gamma = k_\gamma \hat{\mathbf{R}}$  and

$$\begin{aligned} M_{\gamma\alpha}(\mathbf{k}_\gamma, \mathbf{k}_\alpha; E) &= -\frac{\sqrt{\mu_\gamma \mu_\alpha k_\gamma k_\alpha}}{4\pi \hbar^2} \\ &\times \sum_\beta \int d\mathbf{R} \int d\mathbf{R}' e^{-i\mathbf{k}_\gamma \cdot \mathbf{R}} G_{\gamma\beta}(\mathbf{R}, \mathbf{R}'; E) \chi_{\beta\alpha}^\pi(\mathbf{R}', \mathbf{k}_\alpha) . \end{aligned} \quad (2.6)$$

The Born amplitude is obtained by approximating

$$\chi_{\beta\alpha}^\pi(\mathbf{R}, \mathbf{k}_\alpha) \sim \delta_{\beta,\alpha} \left[ e^{i\mathbf{k}_\alpha \cdot \mathbf{R}} + (-1)^{S_\alpha} \mathcal{P}_\alpha e^{-i\mathbf{k}_\alpha \cdot \mathbf{R}} \right] \quad (2.7)$$

in Eq. (2.6). Though  $\mathbf{k}_\alpha$  and  $\mathbf{k}_\gamma$  are related to the total energy  $E$  by the on-shell condition

$$E = E_\gamma^{int} + \frac{\hbar^2}{2\mu_\gamma} \mathbf{k}_\gamma^2 = E_\alpha^{int} + \frac{\hbar^2}{2\mu_\alpha} \mathbf{k}_\alpha^2 , \quad (2.8)$$

it is convenient to relax this condition in order to define a more general Born amplitude. Namely,  $\mathbf{k}_\gamma$  and  $\mathbf{k}_\alpha$  are denoted by  $\mathbf{k}$  and  $\mathbf{k}'$ , respectively, in what follows. Then the Born amplitude reads as<sup>\*)</sup>

$$M_{\gamma\alpha}^{\text{Born}}(\mathbf{k}, \mathbf{k}'; E) = -\frac{\sqrt{\mu_\gamma \mu_\alpha k k'}}{4\pi \hbar^2} \left[ M_{\gamma\alpha}^B(\mathbf{k}, \mathbf{k}'; E) + (-1)^{S_\alpha} \mathcal{P}_\alpha M_{\gamma\alpha}^B(\mathbf{k}, -\mathbf{k}'; E) \right] . \quad (2.9)$$

The Born amplitude Eq. (2.9) has a high degree of symmetries which can be directly derived from those of Eq. (2.3). First  $M_{\gamma\alpha}^{\text{Born}}(\mathbf{k}, \mathbf{k}'; E)$  is a function of  $\mathbf{k}^2$ ,  $\mathbf{k}'^2$  and  $\cos \theta = \hat{\mathbf{k}} \cdot \hat{\mathbf{k}}'$  with real coefficients, and satisfies the symmetry

$$M_{\gamma\alpha}^{\text{Born}}(\mathbf{k}, \mathbf{k}'; E) = M_{\gamma\alpha}^{\text{Born}}(\mathbf{k}, \mathbf{k}'; E)^* = M_{\alpha\gamma}^{\text{Born}}(\mathbf{k}', \mathbf{k}; E) . \quad (2.10)$$

---

<sup>\*)</sup> In Eqs. (2.9), (2.19) and (2.21), the relative energy  $\varepsilon_\gamma$  in the basic Born kernel (in the prior form) should be calculated from the total energy  $E$  through  $\varepsilon_\gamma = E - E_\gamma^{int}$ .

The parity conservation implies

$$\begin{aligned}
M_{\gamma\alpha}^{\text{Born}}(\mathbf{k}, \mathbf{k}'; E) &= M_{\gamma\alpha}^{\text{Born}}(-\mathbf{k}, -\mathbf{k}'; E) \\
&= (-1)^{S_\gamma} \mathcal{P}_\gamma M_{\gamma\alpha}^{\text{Born}}(-\mathbf{k}, \mathbf{k}'; E) \\
&= (-1)^{S_\alpha} \mathcal{P}_\alpha M_{\gamma\alpha}^{\text{Born}}(\mathbf{k}, -\mathbf{k}'; E) \quad , \quad (2.11)
\end{aligned}$$

with  $(-1)^{S_\gamma} \mathcal{P}_\gamma = (-1)^{S_\alpha} \mathcal{P}_\alpha = \pi$ .

We now move to the momentum representation in Eq. (2.4) through

$$\chi_{\gamma\alpha}^\pi(\mathbf{R}, \mathbf{k}_\alpha) = \int d\mathbf{k} e^{i\mathbf{k}\cdot\mathbf{R}} \widehat{\chi}_{\gamma\alpha}^\pi(\mathbf{k}, \mathbf{k}_\alpha) \quad . \quad (2.12)$$

Then Eq. (2.6) is expressed as

$$M_{\gamma\alpha}(\mathbf{k}_\gamma, \mathbf{k}_\alpha; E) = -\frac{\sqrt{\mu_\gamma \mu_\alpha k_\gamma k_\alpha}}{4\pi\hbar^2} \sum_\beta \int d\mathbf{k}' V_{\gamma\beta}(\mathbf{k}_\gamma, \mathbf{k}'; E) \widehat{\chi}_{\beta\alpha}^\pi(\mathbf{k}', \mathbf{k}_\alpha) \quad , \quad (2.13)$$

where the Born kernel  $V_{\gamma\beta}(\mathbf{k}, \mathbf{k}'; E)$  defined by

$$V_{\gamma\beta}(\mathbf{k}, \mathbf{k}'; E) = \frac{1}{2} \left[ M_{\gamma\beta}^B(\mathbf{k}, \mathbf{k}'; E) + (-1)^{S_\beta} \mathcal{P}_\beta M_{\gamma\beta}^B(\mathbf{k}, -\mathbf{k}'; E) \right] \quad (2.14)$$

is related to the Born amplitude through

$$M_{\gamma\alpha}^{\text{Born}}(\mathbf{k}, \mathbf{k}'; E) = -\frac{\sqrt{\mu_\gamma \mu_\alpha k_\gamma k_\alpha}}{2\pi\hbar^2} V_{\gamma\alpha}(\mathbf{k}, \mathbf{k}'; E) \quad (2.15)$$

We write Eq. (2.13) as

$$M_{\gamma\alpha}(\mathbf{k}_\gamma, \mathbf{k}_\alpha; E) = -\frac{\sqrt{\mu_\gamma \mu_\alpha k_\gamma k_\alpha}}{2\pi\hbar^2} T_{\gamma\alpha}(\mathbf{k}_\gamma, \mathbf{k}_\alpha; E) \quad (2.16)$$

and define the on-shell  $T$ -matrix by

$$T_{\gamma\alpha}(\mathbf{k}_\gamma, \mathbf{k}_\alpha; E) = \frac{1}{2} \sum_\beta \int d\mathbf{k}' V_{\gamma\beta}(\mathbf{k}_\gamma, \mathbf{k}'; E) \widehat{\chi}_{\beta\alpha}^\pi(\mathbf{k}', \mathbf{k}_\alpha) \quad . \quad (2.17)$$

Then the momentum representation of Eq. (2.4) reads as

$$\begin{aligned}
\widehat{\chi}_{\gamma\alpha}^\pi(\mathbf{k}, \mathbf{k}_\alpha) &= \delta_{\gamma,\alpha} \left[ \delta(\mathbf{k} - \mathbf{k}_\alpha) + (-1)^{S_\alpha} \mathcal{P}_\alpha \delta(\mathbf{k} + \mathbf{k}_\alpha) \right] \\
&+ \frac{1}{(2\pi)^3} \frac{2\mu_\gamma}{\hbar^2} \frac{1}{k_\gamma^2 - k^2 + i\varepsilon} 2 T_{\gamma\alpha}(\mathbf{k}, \mathbf{k}_\alpha; E) \quad . \quad (2.18)
\end{aligned}$$

If we use Eq. (2.18) in Eq. (2.17) and release the on-shell condition Eq. (2.8), we finally obtain

$$\begin{aligned}
T_{\gamma\alpha}(\mathbf{p}, \mathbf{q}; E) &= V_{\gamma\alpha}(\mathbf{p}, \mathbf{q}; E) + \sum_\beta \frac{1}{(2\pi)^3} \int d\mathbf{k} V_{\gamma\beta}(\mathbf{p}, \mathbf{k}; E) \\
&\times \frac{2\mu_\beta}{\hbar^2} \frac{1}{k_\beta^2 - k^2 + i\varepsilon} T_{\beta\alpha}(\mathbf{k}, \mathbf{q}; E) \quad , \quad (2.19)
\end{aligned}$$

which we call an LS-RGM equation.

The partial-wave decomposition of the scattering amplitudes etc. are carried out in the standard way<sup>18)</sup>. For example, we have <sup>\*</sup>)

$$T_{\gamma\alpha}(\mathbf{k}, \mathbf{k}'; E) = \sum'_{JM\ell\ell'} 4\pi T_{\gamma S'\ell', \alpha S\ell}^J(k, k'; E) \\ \times \sum_{m'} \langle \ell' m' S' S'_z | JM \rangle Y_{\ell' m'}(\hat{\mathbf{k}}) \sum_m \langle \ell m S S_z | JM \rangle Y_{\ell m}^*(\hat{\mathbf{k}}') \quad , \quad (2.20)$$

where  $\gamma = [1/2(11)c_1, 1/2(11)c_2] S' S'_z Y I I_z; \mathcal{P}'$ . The prime on the summation symbol indicates that  $\ell$  ( $\ell'$ ) is limited to such values that satisfy the condition  $(-1)^\ell = (-1)^{S\mathcal{P}}$  ( $(-1)^{\ell'} = (-1)^{S'\mathcal{P}'}$ ). We write the spin quantum numbers  $S$  and  $S'$  of the  $T$ -matrix explicitly for the later convenience, although these are already included in the definition of  $\alpha$  and  $\gamma$ . The partial-wave decomposition of the LS-RGM equation yields

$$T_{\gamma S'\ell', \alpha S\ell}^J(p, q; E) = V_{\gamma S'\ell', \alpha S\ell}^J(p, q; E) + \sum'_{\beta S''\ell''} \frac{4\pi}{(2\pi)^3} \int_0^\infty k^2 dk \\ \times V_{\gamma S'\ell', \beta S''\ell''}^J(p, k; E) \frac{2\mu_\beta}{\hbar^2} \frac{1}{k_\beta^2 - k^2 + i\varepsilon} T_{\beta S''\ell'', \alpha S\ell}^J(k, q; E) \quad , \quad (2.21)$$

where  $E = E_\beta^{int} + (\hbar^2/2\mu_\beta)\mathbf{k}_\beta^2$  and  $V_{\gamma S'\ell', \alpha S\ell}^J(p, q; E)$  is the partial-wave decomposition of  $V_{\gamma\alpha}(\mathbf{p}, \mathbf{q}; E)$ . The Lippmann-Schwinger equation Eq. (2.21) involves a pole at  $k = k_\beta$  in the Green function. A proper treatment of such a singularity for positive energies is well known in the field of few-body problems.<sup>13), 14), 20)</sup> Here we use the technique developed by Noyes<sup>13)</sup> and Kowalski<sup>14)</sup>, and separate the momentum region of  $k$  (and also  $p$  and  $q$ ) into two pieces. After eliminating the singularity, we carry out the integral over  $0 \leq k \leq k_\beta$  by the Gauss-Legendre 15-point quadrature formula, and the integral over  $k_\beta \leq k < \infty$  by using the Gauss-Legendre 20-point quadrature formula through the mapping,  $k = k_\beta + \tan(\pi/4)(1 + x)$ .

## 2.2. Basic Born kernel

In this subsection we explain how to obtain the basic Born kernel, Eq. (2.3), in detail. In fact the calculation of the kernel is rather tedious and a careful check of the calculation must be made. Recent modern techniques, especially developed in the microscopic nuclear cluster theory of light nuclei<sup>21), 22), 23)</sup>, have greatly reduced the labor of tedious calculations. Since two-body forces used in such applications are usually momentum-independent central and spin-orbit forces of the Gaussian radial dependence, one needs to extend the technique to more general two-body forces involving various types of the tensor forces and Yukawa functions<sup>24), 25)</sup>. Appendix

---

<sup>\*</sup>) In this paper we use the phase convention of the  $S$ -matrix defined through the partial wave decomposition in terms of the time reversal state  $i^\ell Y_{\ell m}(\hat{\mathbf{r}})$  in the coordinate space. This phase convention is different from the standard one by Blatt and Biedenharn<sup>19)</sup> by the factor  $i^{\ell-\ell'}$ , and introduces an extra minus sign for the mixing parameter  $\epsilon_J$  for the  $NN$  scattering. Similarly, all the Pauli-spinor invariants in Eq. (2.29) are taken to be “real” operators<sup>17)</sup>.

A gives a very general formula to calculate the Born kernel directly from such two-body forces by simple Gaussian integrations.

Another important technical development in our quark-model approach to the  $NN$  and  $YN$  interactions is motivated by the rich flavor contents of the spin-flavor  $SU_6$  wave functions of baryons. The operator formalism introduced in Refs. 26) and 27) makes it possible to represent this flavor dependence in a transparent form by using abstract  $SU_3$  operators expressed by the basic electric- and magnetic-type  $SU_6$  unit vectors. This formalism is also useful to deal with the flavor symmetry breaking.<sup>\*)</sup>

Keeping in mind the operator formalism of spin-flavor factors, we can express the basic Born kernel in Eq. (2.3) as

$$\begin{aligned} M^B(\mathbf{q}_f, \mathbf{q}_i; E) &= \langle e^{i\mathbf{q}_f \cdot \mathbf{R}} | G(\mathbf{R}, \mathbf{R}'; E) | e^{i\mathbf{q}_i \cdot \mathbf{R}'} \rangle \\ &= M_D^{CN}(\mathbf{q}_f, \mathbf{q}_i) + M_D^{SN}(\mathbf{q}_f, \mathbf{q}_i) + M_D^{TN}(\mathbf{q}_f, \mathbf{q}_i) S_{12}(\mathbf{k}, \mathbf{k}) \\ &\quad + \sum_{\Omega} M^{\Omega}(\mathbf{q}_f, \mathbf{q}_i) \mathcal{O}^{\Omega}(\mathbf{q}_f, \mathbf{q}_i) - \varepsilon M_N(\mathbf{q}_f, \mathbf{q}_i) \quad , \quad (2.22) \end{aligned}$$

where  $\varepsilon$  is the relative energy in the final channel (in the prior form) when the channel matrix elements are taken at the baryon level. Each component of the Born kernel Eq. (2.22) is given in Appendix B in terms of the transferred momentum  $\mathbf{k} = \mathbf{q}_f - \mathbf{q}_i$  and the local momentum  $\mathbf{q} = (\mathbf{q}_f + \mathbf{q}_i)/2$ . In Eq. (2.22) the space-spin invariants  $\mathcal{O}^{\Omega} = \mathcal{O}^{\Omega}(\mathbf{q}_f, \mathbf{q}_i)$  are given by  $\mathcal{O}^{central} = 1$  and<sup>\*\*)</sup>

$$\begin{aligned} \mathcal{O}^{LS} &= i\mathbf{n} \cdot \mathbf{S} \quad , \quad \mathcal{O}^{LS^{(-)}} = i\mathbf{n} \cdot \mathbf{S}^{(-)} \quad , \quad \mathcal{O}^{LS^{(-)\sigma}} = i\mathbf{n} \cdot \mathbf{S}^{(-)} P_{\sigma} \quad , \\ \text{with } \mathbf{n} &= [\mathbf{q}_i \times \mathbf{q}_f] \quad , \quad \mathbf{S} = \frac{1}{2}(\boldsymbol{\sigma}_1 + \boldsymbol{\sigma}_2) \quad , \quad \mathbf{S}^{(-)} = \frac{1}{2}(\boldsymbol{\sigma}_1 - \boldsymbol{\sigma}_2) \quad , \\ \text{and } P_{\sigma} &= \frac{1 + \boldsymbol{\sigma}_1 \cdot \boldsymbol{\sigma}_2}{2} \quad . \quad (2.23) \end{aligned}$$

For the tensor part, it would be convenient to take three natural operators defined by

$$\mathcal{O}^T = S_{12}(\mathbf{k}, \mathbf{k}) \quad , \quad \mathcal{O}^{T'} = S_{12}(\mathbf{q}, \mathbf{q}) \quad , \quad \mathcal{O}^{T''} = S_{12}(\mathbf{k}, \mathbf{q}) \quad , \quad (2.24)$$

where  $S_{12}(\mathbf{a}, \mathbf{b}) = (3/2)[(\boldsymbol{\sigma}_1 \cdot \mathbf{a})(\boldsymbol{\sigma}_2 \cdot \mathbf{b}) + (\boldsymbol{\sigma}_2 \cdot \mathbf{a})(\boldsymbol{\sigma}_1 \cdot \mathbf{b})] - (\boldsymbol{\sigma}_1 \cdot \boldsymbol{\sigma}_2)(\mathbf{a} \cdot \mathbf{b})$ . The invariant Born kernel  $M^{\Omega}(\mathbf{q}_f, \mathbf{q}_i)$  in Eq. (2.22) consists of various types of spin-flavor factors  $X_{\mathcal{T}}^{\Omega}$  and the spatial functions  $f_{\mathcal{T}}^{\Omega}(\theta)$  calculated for the quark-exchange kernel of the FB interaction.<sup>\*\*\*)</sup> It is explicitly given in Appendix B and is generally expressed as

$$M^{\Omega}(\mathbf{q}_f, \mathbf{q}_i) = \sum_{\mathcal{T}} X_{\mathcal{T}}^{\Omega} f_{\mathcal{T}}^{\Omega}(\theta) \quad . \quad (2.25)$$

Here we should note that the spin-flavor factors depend on the isospin and that the spatial function  $f_{\mathcal{T}}^{\Omega}(\theta)$  is actually a function of  $\mathbf{q}_f^2, \mathbf{q}_i^2$  and the relative angle  $\theta$ :  $\cos \theta =$

<sup>\*)</sup> The full account of the operator formalism for the spin-flavor factors of the RGM kernel will be published elsewhere.

<sup>\*\*)</sup> Here we use a slightly different notation for  $\Omega$  from that used in § 2.1, but the correspondence is almost apparent.

<sup>\*\*\*)</sup> Here we will show only the expressions for the quark sector. Those for the EMEP sector are easily obtained by some trivial modifications.



$\hat{\mathbf{q}}_f \cdot \hat{\mathbf{q}}_i$ . The sum over  $\mathcal{T}$  in Eq. (2·25) is with respect to the quark-exchange interaction types<sup>23)</sup>  $\mathcal{T} = E, S, S', D_+$  and  $D_-$ . The factors  $X_E^\Omega$  (possible only for the central force) should be replaced with  $-X_{S'}^\Omega$ , because of the subtraction of the internal-energy contribution in the prior form. Finally the partial-wave decomposition of the Born kernel,  $V_{S'\ell',S\ell}^{J\Omega}(q_f, q_i)$  can be calculated by using<sup>\*)</sup>

$$f_{\mathcal{T}\ell}^\Omega = \frac{1}{2} \int_{-1}^1 f_{\mathcal{T}}^\Omega(\theta) P_\ell(\cos\theta) d(\cos\theta) \quad , \quad (2\cdot26)$$

as follows:

$$V_{S'\ell',S\ell}^{J \text{ central } \Omega}(q_f, q_i) = \delta_{\ell',\ell} \delta_{S',S} \sum_{\mathcal{T}} X_{\mathcal{T}}^\Omega f_{\mathcal{T}\ell}^\Omega \quad \text{with} \quad (\boldsymbol{\sigma}_1 \cdot \boldsymbol{\sigma}_2) = 2S(S+1) - 3 \quad ,$$

$$V_{S'\ell',S\ell}^{J \text{ LS}}(q_f, q_i) = \delta_{\ell',\ell} \delta_{S',S} \delta_{S,1} q_f q_i \frac{1}{2(2\ell+1)} [\ell(\ell+1) + 2 - J(J+1)] \\ \times \sum_{\mathcal{T}} X_{\mathcal{T}}^{LS} (f_{\mathcal{T}\ell+1}^{LS} - f_{\mathcal{T}\ell-1}^{LS}) \quad ,$$

$$\left. \begin{array}{l} V_{S'\ell',S\ell}^{J \text{ LS}^{(-)}}(q_f, q_i) \\ V_{S'\ell',S\ell}^{J \text{ LS}^{(-)\sigma}}(q_f, q_i) \end{array} \right\} = \left\{ \begin{array}{l} -1 \\ (-1)^S \end{array} \right\} \delta_{\ell',\ell} \delta_{J,\ell} q_f q_i \frac{\sqrt{J(J+1)}}{2J+1} \\ \times \sum_{\mathcal{T}} \left\{ \begin{array}{l} X_{\mathcal{T}}^{LS^{(-)}} \\ X_{\mathcal{T}}^{LS^{(-)\sigma}} \end{array} \right\} (f_{\mathcal{T}J+1}^{LS} - f_{\mathcal{T}J-1}^{LS}) \quad \text{for} \quad S, S = 1, 0 \text{ or } 0, 1 \quad ,$$

$$V_{S'\ell',S\ell}^{J \text{ T total}}(q_f, q_i) = \delta_{S',S} \delta_{S,1} (S_{12})_{\ell',\ell}^J \\ \times \left[ q_f^2 V_\ell^{T(ff)} + q_i^2 V_{\ell'}^{T(ii)} + q_f q_i \left\{ \frac{1}{2\ell+1} \left[ \left( \ell - \frac{1}{2} \right) V_{\ell+1}^{T(fi)} + \left( \ell + \frac{3}{2} \right) V_{\ell-1}^{T(fi)} \right] \right\} \right] \\ \text{for} \quad \left\{ \begin{array}{l} \ell' = \ell \pm 2 \quad \text{and} \quad J = \ell \pm 1 \\ \ell = \ell' = J, \quad J \pm 1 \end{array} \right. \quad . \quad (2\cdot27)$$

Here the tensor component is the sum over  $\Omega = T, T'$  and  $T''$  and

$$\left. \begin{array}{l} V_\ell^{T(ff)} \\ V_\ell^{T(ii)} \end{array} \right\} = \left\{ \begin{array}{l} 9 \\ 1 \end{array} \right\} \frac{1}{4} X_S^T f_{S\ell}^T + \left\{ \begin{array}{l} 1 \\ 9 \end{array} \right\} \frac{1}{4} X_{S'}^T f_{S'\ell}^T + X_{D_+}^T f_{D_+\ell}^T + \frac{1}{4} X_{D_-}^T f_{D_-\ell}^T \quad , \\ V_\ell^{T(fi)} = -\frac{3}{2} \left[ X_S^T f_{S\ell}^T + X_{S'}^T f_{S'\ell}^T \right] - 2X_{D_+}^T f_{D_+\ell}^T + \frac{1}{2} X_{D_-}^T f_{D_-\ell}^T \quad . \quad (2\cdot28)$$

Furthermore,  $(S_{12})_{\ell',\ell}^J$  is the standard tensor factor. In Eqs. (2·25), (2·27) and (2·28), the spin-flavor factors  $X_{\mathcal{T}}^\Omega$  should be replaced with  $X_{x=1\mathcal{T}}^\Omega$  for the EMEP exchange terms,  $\Omega = CN, SN$  and  $TN$ . Also, the direct term with  $x = 0$  is possible only for  $\mathcal{T} = D_+$ .

### 2.3. Invariant amplitudes

Since the three vectors,  $\mathbf{k} = \mathbf{q}_f - \mathbf{q}_i$ ,  $\mathbf{q} = (\mathbf{q}_f + \mathbf{q}_i)/2$  and  $\mathbf{n} = \mathbf{q}_i \times \mathbf{q}_f = \mathbf{q} \times \mathbf{k}$  are not mutually orthogonal for the  $YN$  interaction, we use  $\mathbf{k} = \mathbf{q}_f - \mathbf{q}_i$ ,  $\mathbf{n} = \mathbf{q} \times \mathbf{k}$

<sup>\*)</sup> We use the Gauss-Legendre 20-point quadrature formula to carry out the numerical integration of Eq. (2·26) over  $\cos\theta = -1 \sim 1$ .

and  $\mathbf{P} = \mathbf{k} \times \mathbf{n} = \mathbf{k}^2 \mathbf{q} - (\mathbf{k} \cdot \mathbf{q}) \mathbf{k}$  to define the invariant amplitudes of Eq. (2.13):

$$\begin{aligned}
M(\mathbf{q}_f, \mathbf{q}_i; E) &= g_0 + h_0 i(\boldsymbol{\sigma}_1 + \boldsymbol{\sigma}_2) \cdot \hat{\mathbf{n}} + h_- i(\boldsymbol{\sigma}_1 - \boldsymbol{\sigma}_2) \cdot \hat{\mathbf{n}} \\
&+ h_n (\boldsymbol{\sigma}_1 \cdot \hat{\mathbf{n}}) \cdot (\boldsymbol{\sigma}_2 \cdot \hat{\mathbf{n}}) + h_k (\boldsymbol{\sigma}_1 \cdot \hat{\mathbf{k}}) \cdot (\boldsymbol{\sigma}_2 \cdot \hat{\mathbf{k}}) + h_P (\boldsymbol{\sigma}_1 \cdot \hat{\mathbf{P}}) \cdot (\boldsymbol{\sigma}_2 \cdot \hat{\mathbf{P}}) \\
&+ f_+ \left\{ (\boldsymbol{\sigma}_1 \cdot \hat{\mathbf{k}})(\boldsymbol{\sigma}_2 \cdot \hat{\mathbf{P}}) + (\boldsymbol{\sigma}_1 \cdot \hat{\mathbf{P}})(\boldsymbol{\sigma}_2 \cdot \hat{\mathbf{k}}) \right\} \\
&+ f_- \left\{ (\boldsymbol{\sigma}_1 \cdot \hat{\mathbf{k}})(\boldsymbol{\sigma}_2 \cdot \hat{\mathbf{P}}) - (\boldsymbol{\sigma}_1 \cdot \hat{\mathbf{P}})(\boldsymbol{\sigma}_2 \cdot \hat{\mathbf{k}}) \right\} .
\end{aligned} \tag{2.29}$$

The eight invariant amplitudes,  $g_0, \dots, f_-$ , are complex functions of the total energy  $E$  and the scattering angle,  $\cos \theta = \hat{\mathbf{q}}_i \cdot \hat{\mathbf{q}}_f$ . Three of the eight invariant amplitudes,  $h_-$ ,  $f_+$  and  $f_-$ , do not appear for the  $NN$  scattering due to the identity of two particles ( $h_-$  and  $f_-$ ) and the time-reversal invariance ( $f_-$  and  $f_+$ ). These three terms correspond to the non-central forces characteristic in the  $YN$  scattering; i.e.,  $h_-$  corresponds to  $LS^{(-)}$ ,  $f_+$  to  $S_{12}(\mathbf{r}, \mathbf{p})$ , and  $f_-$  to  $LS^{(-)}\sigma$ , respectively.<sup>17)</sup> In particular, the antisymmetric  $LS$  interactions,  $LS^{(-)}$  and  $LS^{(-)}\sigma$ , involve the spin change between 0 and 1, together with the transition of the flavor-exchange symmetry  $\mathcal{P} \neq \mathcal{P}'$ . In the  $NN$  scattering this process is not allowed, since the flavor-exchange symmetry is uniquely specified by the conserved isospin:  $\mathcal{P} = (-1)^{1-I}$ . On the contrary, these interactions are in general all possible in the  $YN$  scattering, which gives an intriguing interplay of non-central forces.

The invariant amplitudes are expressed by the  $S$ -matrix elements through the partial-wave decomposition of the scattering amplitude Eq. (2.13). If we write it as

$$\begin{aligned}
M_{\gamma\alpha}(\mathbf{q}_f, \mathbf{q}_i; E) &= \sum_{JM\ell\ell'}^J 4\pi R_{\gamma S'\ell', \alpha S\ell}^J \\
&\times \sum_{m'} \langle \ell' m' S' S'_z | JM \rangle Y_{\ell' m'}(\hat{\mathbf{q}}_f) \sum_m \langle \ell m S S_z | JM \rangle Y_{\ell m}^*(\hat{\mathbf{q}}_i) ,
\end{aligned} \tag{2.30}$$

the partial-wave component  $R_{\gamma S'\ell', \alpha S\ell}^J = (1/2i)(S_{\gamma S'\ell', \alpha S\ell}^J - \delta_{\gamma, \alpha} \delta_{S', S} \delta_{\ell', \ell})$  is obtained from the relationship in Eq. (2.16):

$$R_{\gamma S'\ell', \alpha S\ell}^J = -\frac{\sqrt{\mu_\gamma \mu_\alpha q_f q_i}}{2\pi \hbar^2} T_{\gamma S'\ell', \alpha S\ell}^J(q_f, q_i; E) \tag{2.31}$$

where  $\varepsilon_\gamma = (\hbar^2/2\mu_\gamma)q_f^2$ ,  $\varepsilon_\alpha = (\hbar^2/2\mu_\alpha)q_i^2$  and  $E = E_\gamma^{int} + \varepsilon_\gamma = E_\alpha^{int} + \varepsilon_\alpha$ . The formulae given in Appendix D are then used to reconstruct the invariant amplitudes by the solution of the LS-RGM equation Eq. (2.21). All the scattering observables are expressed in terms of these invariant amplitudes. For example, the differential cross section and the polarization of the scattered particle are given by

$$\begin{aligned}
\frac{d\sigma}{d\Omega} &= \sigma_0(\theta) = |g_0|^2 + |h_0 + h_-|^2 + |h_0 - h_-|^2 , \\
&+ |h_n|^2 + |h_k|^2 + |h_P|^2 + |f_+ + f_-|^2 + |f_+ - f_-|^2 \\
P(\theta) &= 2\Im m [g_0(h_0 + h_-)^* + h_n(h_0 - h_-)^*] \\
&+ 2\Im m [h_k(f_+ - f_-)^* - h_P(f_+ + f_-)^*] .
\end{aligned} \tag{2.32}$$

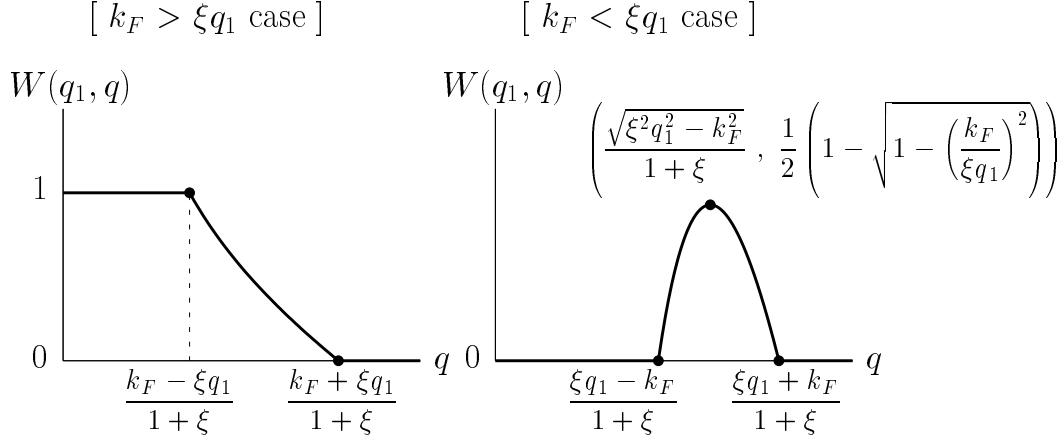


Fig. 1. The weight function  $W(q_1, q)$  in Eq. (2.37) as a function of  $q$ .

#### 2.4. $t^{eff} \rho$ prescription for single-particle potentials

In this subsection we will derive an approximate formula to calculate s.p. potentials appearing in the lowest-order Brueckner theory. The Bethe-Goldstone (BG) equation for the  $G$ -matrix solution is given by<sup>15)</sup>

$$G_{\gamma S' \ell', \alpha S \ell}^J(p, q; K, \omega) = V_{\gamma S' \ell', \alpha S \ell}^J(p, q; E) + \sum'_{\beta S'' \ell''} \frac{4\pi}{(2\pi)^3} \int_0^\infty k^2 dk$$

$$\times V_{\gamma S' \ell', \beta S'' \ell''}^J(p, k; E) \frac{Q_\beta(k, K)}{e_\beta(k, K; \omega)} G_{\beta S'' \ell'', \alpha S \ell}^J(k, q; K, \omega) . \quad (2.33)$$

where we assume  $E = E_\alpha^{int} + (\hbar^2/2\mu_\alpha)q^2$ . In Eq. (2.33),  $Q_\beta(k, K)$  stands for the angle-averaged Pauli operator and  $e_\beta(k, K; \omega)$  is the energy denominator given by<sup>\*)</sup>

$$e_\beta(k, K; \omega) = \omega - E_b(k_1) - E_N(k_2) , \quad (2.34)$$

with the s.p. energy  $E_b(k)$ :

$$E_b(k) = M_b + \frac{\hbar^2}{2M_b} k^2 + U_b(k) . \quad (2.35)$$

The s.p. potential  $U_b(k)$  is calculated from

$$U_a(q_1) = (1 + \delta_{a,N})(1 + \xi)^3 \sum_I \frac{2I + 1}{2(2I_a + 1)}$$

$$\times \sum_{J \ell S} (2J + 1) \frac{1}{2\pi^2} \int_0^{q_{max}} q^2 dq W(q_1, q) G_{a S \ell, a S \ell}^J(q, q; K, \omega) , \quad (2.36)$$

where  $q_{max} = (k_F + \xi q_1)/(1 + \xi)$  with  $\xi = (M_N/M_a)$  and  $W(q_1, q)$  is the phase space factor given by

$$W(q_1, q) = \frac{1}{2} (1 - [-1|x_0|1]) , \quad x_0 = \frac{\xi^2 q_1^2 + (1 + \xi)^2 q^2 - k_F^2}{2\xi(1 + \xi)q_1 q} , \quad (2.37)$$

<sup>\*)</sup> For s.p. potentials, we use the notation  $b_1 = b$  and  $a_1 = a$  to specify baryons.

with  $[a|b|c] \equiv \max(a, \min(b, c))$ <sup>28)</sup>. The profile of  $W(q_1, q)$  is illustrated in Fig. 1. The starting energy  $\omega$  in Eq. (2.34) is a sum of the s.p. energies of two interacting baryons:

$$\begin{aligned} \omega &= E_a(q_1) + E_N(q_2) \\ &= M_a + M_N + \frac{\hbar^2}{2(M_a + M_N)} K^2 + \frac{\hbar^2}{2\mu_\alpha} q^2 + U_a(q_1) + U_N(q_2) \quad , \quad (2.38) \end{aligned}$$

where  $\mathbf{K}$  and  $\mathbf{q}$  are the total and relative momenta corresponding to the initial s.p. momenta  $\mathbf{q}_1$  and  $\mathbf{q}_2$ . Once  $q_1$  and  $q$  are given, the values of  $K$  and  $\omega$  in Eq. (2.36) are calculated through

$$\begin{aligned} K &= (1 + \xi) \left[ q_1^2 + q^2 - q_1 q (1 + [-1|x_0|1]) \right]^{\frac{1}{2}} \quad , \\ q_2 &= \left[ \frac{\xi}{1 + \xi} K^2 + (1 + \xi) q^2 - \xi q_1^2 \right]^{\frac{1}{2}} \quad , \\ \omega &= E_a(q_1) + E_N(q_2) \quad . \end{aligned} \quad (2.39)$$

Let us specialize the system to  $NN$  and consider the asymptotic behavior of the s.p. potential  $U_N(q_1)$  in symmetric nuclear matter. When  $q_1$  is sufficiently large, the weight function  $W(q_1, q)$  shows a delta-function like behavior around  $q = q_1/2$  with respect to the variable  $q$ . (See Fig. 1.) We can replace the  $G$ -matrix in Eq. (2.36) with the one evaluated at  $q = q_1/2$ , and carry out the integration over  $q$  by

$$\int_0^{q_{max}} q^2 dq W(q_1, q) = \frac{k_F^3}{3} \frac{1}{(1 + \xi)^3} \quad . \quad (2.40)$$

On the other hand, the  $G$ -matrix equation Eq. (2.33) for  $q \rightarrow \infty$  should approach the LS-RGM equation Eq. (2.21), since the Pauli operator  $Q_\beta(k, K)$  plays a minor role in such a high momentum region, and the s.p. potentials in the energy denominator  $e_\beta(k, K; \omega)$  is relatively unimportant in comparison with the large kinetic energies. Thus we can expect that the s.p. potential in the high momentum region is well approximated by a product of the on-shell  $T$ -matrix with  $q = q_1/2$  and the density of nuclear matter, which is related to the Fermi momentum  $k_F$  with  $\rho = (2/3\pi^2) k_F^3$ . It should be noted that only the spin-isospin independent part of the  $T$ -matrix contributes, since we take spin-isospin sum for the target nucleons. If we note the relationship Eq. (2.31) and use the partial-wave decomposition of the invariant amplitude  $g_0$  given in Eq. (D.2), we can easily show

$$U_N(q_1) = \frac{1}{4} U_N^0(q_1) + \frac{3}{4} U_N^1(q_1) \quad \text{with} \quad U_N^I(q_1) = 2\rho g_0^I(q = q_1/2, \theta = 0) \quad , \quad (2.41)$$

except for the overall factor  $-(2\pi\hbar^2/\mu q)$ . This relationship is also shown in terms of  $np$  and  $pp$  invariant amplitudes:

$$\begin{aligned} U_N(q_1) &= (\rho/2) \left( g_0^0(q_1/2, 0) + g_0^1(q_1/2, 0) \right) + (\rho/2) 2g_0^1(q_1/2, 0) \\ &= (\rho/2) (g_0^{np}(q_1/2, 0) + g_0^{pp}(q_1/2, 0)) \quad , \end{aligned} \quad (2.42)$$

Table I. Comparison of the phase-shift values and mixing angles (in degree), calculated by the LS-RGM formalism (lseq) and the improved variational method (var), for the  $AN$   ${}^3S_1$ - ${}^3D_1$  -  $\Sigma N$   ${}^3S_1$ - ${}^3D_1$  (upper) and  $AN$   ${}^1P_1$ - ${}^3P_1$  -  $\Sigma N$   ${}^1P_1$ - ${}^3P_1$  (lower) coupled-channel problems. The mixing angles,  $\epsilon_1$  and  $\rho_1$ , are only approximately defined for the energies above the  $\Sigma N$  threshold. The phase convention of  $\epsilon_1$  is the standard one for the bar phase shifts. The model is RGM-F<sup>4)</sup>.

$p_A$		$AN$		$\Sigma N$		$AN$
		${}^3S_1$	${}^3D_1$	${}^3S_1$	${}^3D_1$	$\epsilon_1$
430	lseq	37.494	8.656	–	–	13.802
	var	37.559	8.654	–	–	13.814
	diff	–0.065	0.002	–	–	–0.012
440	lseq	49.169	15.227	–	–	22.999
	var	49.263	15.212	–	–	23.016
	diff	–0.094	0.017	–	–	–0.017
450	lseq	12.831	–5.535	122.619	–0.014	–21.090
	var	12.825	–5.528	122.708	–0.011	–21.099
	diff	0.006	–0.007	–0.089	–0.003	0.009
460	lseq	14.793	–4.461	87.265	–0.165	–13.440
	var	14.801	–4.458	87.298	–0.152	–13.449
	diff	–0.008	–0.003	–0.033	–0.013	0.009

$p_A$		$AN$		$\Sigma N$		$AN$
		${}^1P_1$	${}^3P_1$	${}^1P_1$	${}^3P_1$	$\rho_1$
300	lseq	9.161	5.195	–	–	–8.213
	var	9.161	5.188	–	–	–8.208
	diff	0.000	0.007			–0.005
400	lseq	82.874	0.757	–	–	–41.647
	var	82.605	0.971	–	–	–41.636
	diff	0.269	–0.214	–	–	–0.011
500	lseq	–15.697	–20.945	–1.812	–8.113	16.559
	var	–15.690	–20.944	–1.812	–8.120	16.563
	diff	–0.007	–0.001	0.000	0.007	–0.004
600	lseq	–14.077	–21.357	–5.725	–22.826	13.399
	var	–14.070	–21.358	–5.724	–22.831	13.401
	diff	–0.007	0.001	–0.001	0.005	–0.002

where  $\rho/2$  is the proton and neutron density. This implies that the asymptotic behavior of the s.p. potential in the high momentum region is determined by the values of the spin-independent central invariant amplitudes at the forward angle. This rule is called  $t^{eff}\rho$  prescription, which is sometimes used in the relativistic mean field theory. For example, if we want to calculate  $U_N(q_1)$  for  $q_1 = 6.210\text{fm}^{-1}$

in nuclear matter of the normal density with  $k_F = 1.35 \text{ fm}^{-1}$  ( $\rho = (2/3\pi^2)k_F^3 = 0.1662 \text{ fm}^{-3}$ ), we only need to derive the invariant amplitude ( $g_0^0(\theta = 0) + 3g_0^1(\theta = 0)$ ) for  $T_{lab} = 800 \text{ MeV}$  ( $q = q_1/2 = 3.105 \text{ fm}^{-1}$ ) and multiply it by the factor,  $-(4\pi/q)(\hbar^2/M_N)(\rho/2) = -(4\pi/3.105) \cdot 41.47 \cdot 0.0831 = -13.95$ .

### §3. Comparison with the improved variational method

As a check of the LS-RGM formalism, we consider the phase-shift parameters of the  $\Lambda N$ - $\Sigma N(I = 1/2)$  coupled-channel system, and compare them with the predictions by the improved variational method. Here we consider two different types of the  $\Lambda N$ - $\Sigma N(I = 1/2)$  couplings. The first one is the  ${}^3S_1$ - ${}^3D_1$  channel coupling by the tensor force, which dominantly comes from the EMEP, especially, from the one-pion exchange tensor force. The other is the  ${}^1P_1$  -  ${}^3P_1$  coupling by the  $LS^{(-)}$  force originating from the FB interaction. Since the quark model usually predicts very strong  $LS^{(-)}$  force, the  $\Lambda p$  scattering observables involve very rich information on the characters of the non-central forces in the  $YN$  interaction.

Table I shows a comparison between the phase-shift values predicted by the LS-RGM formalism (lseq) and the improved variational method (var) with respect to the  $\Lambda N$   ${}^3S_1$ - ${}^3D_1$ - $\Sigma N$   ${}^3S_1$ - ${}^3D_1$  (upper) and  $\Lambda N$   ${}^1P_1$ - ${}^3P_1$ - $\Sigma N$   ${}^1P_1$ - ${}^3P_1$  (lower) coupled-channel problems. The mixing angle  $\epsilon_1$  ( $\rho_1$ ) between the  ${}^3S_1$  and  ${}^3D_1$  ( ${}^1P_1$  and  ${}^3P_1$ ) channels of  $\Lambda N$  is also compared. The model is RGM-F<sup>4)</sup>, which gives the  $\Sigma N$  threshold energy at  $p_A = 445 \text{ MeV}/c$ . In spite of the prominent resonance behavior in this energy region, the two methods give very similar values for the phase shifts. The difference (diff) is less than  $0.1^\circ$  for the  ${}^3S_1$ - ${}^3D_1$  coupling. For the  ${}^1P_1$ - ${}^3P_1$  coupling, we find that the accuracy deteriorates because of the strong resonance in the  $\Lambda N$   ${}^1P_1$  channel. If we avoid this energy region, the accuracy is very good. The difference is usually less than  $0.01^\circ$ .

Since the resonance behavior in the above two coupled-channel systems is largely model-dependent, we summarize it in Table II for the three versions of our quark model. Here  $V_{\Sigma N(I=1/2)}^C({}^3S)$  indicates the strength of the central attraction in the  $\Sigma N(I = 1/2)$  channel, which is evaluated from the  ${}^3S$  effective potential obtained through the  $\mathbf{p} = 0$  Wigner transform of the exchange kernel. We find that the  $\Lambda N$   ${}^3S_1$  resonance in RGM-F appears as a cusp, when the attraction of the  $\Sigma N(I = 1/2)$  channel is not strongly attractive as in FSS and RGM-H. Similarly, the  $\Sigma N(I = 1/2)$   ${}^3P_1$  resonance does not move to the  $\Lambda N$   ${}^1P_1$  state in RGM-H, which has the weakest central attraction in the  $\Sigma N(I = 1/2)$  channel among our three models.

### §4. $NN$ invariant amplitudes at intermediate energies

Figures 2 and 3 compare with the experimental data<sup>29)</sup> the model predictions of the elastic differential cross sections and the polarizations for the the  $np$  and  $pp$  scattering in the  $T_{lab} = 400 \sim 800 \text{ MeV}$  range. These observables in the lower energies are given in Ref. 7). The model in Fig. 2 is FSS for the  $np$  scattering, and that in Fig. 3 is RGM-H for the  $pp$  scattering. The Coulomb force for the  $pp$  scattering

Table II. Resonance behavior near the  $\Sigma N$  threshold for the  $I = 1/2$  states, predicted by RGM-F<sup>4)</sup>, FSS<sup>5), 6)</sup> and RGM-H<sup>6)</sup>. “step” denotes the step-like resonance and “disp” the dispersion-like resonance.

model	RGM-F	FSS	RGM-H
$E_{\Sigma N}^{th}$ (MeV)	39	77	77
$V_{\Sigma N(1/2)}^C(^3S)$	-38	-24	-18
$\Lambda N$ $^3S_1$	step	cusp	cusp
$\Lambda N$ $^3D_1$	disp	disp	disp
$\Sigma N$ $^3S_1$	$\delta = 180^\circ \downarrow$	$\delta \lesssim 60^\circ$	$\delta \lesssim 45^\circ$
$\Sigma N$ $^3D_1$	$\delta \lesssim 0$	$\delta \lesssim 0$	$\delta \lesssim 0$
$\Lambda N$ $^1P_1$	step	step	disp
$\Lambda N$ $^3P_1$	disp	disp	disp
$\Sigma N$ $^1P_1$	$\delta \lesssim 0$	$\delta \lesssim 0$	$\delta \sim 0 \rightarrow 60^\circ$
$\Sigma N$ $^3P_1$	$\delta < 0$	$\delta \lesssim 0$	$\delta \lesssim 40^\circ$

is neglected, since it only affects the extreme forward and backward angles in this high energy region. The solid curve indicates the predictions obtained by solving the LS-RGM equation, while the dashed curve the results of the Born approximation. The latter approximation is apparently inappropriate even at these high energies. However, it is outstanding that the calculated Born invariant amplitudes, leading to these cross sections in the Born approximation, have almost the same order of magnitude as the empirical amplitudes determined from the phase-shift analysis<sup>29)</sup>. Note that the polarization vanishes in the Born approximation. In these calculations no imaginary potential is introduced. The theory overestimates the  $np$  differential cross sections at backward angles. The  $np$  polarization has an unpleasant oscillation around  $\theta_{c.m.} \sim 110^\circ$ . There appears a symmetry in the  $pp$  scattering because of the identity of two protons: The differential cross section becomes symmetric with respect to  $\theta_{c.m.} = 90^\circ$ , and the polarization is symmetric with an opposite sign. The  $pp$  polarization for  $T_{lab} \geq 400$  MeV shows an oscillation around  $90^\circ$ , which is not present in the experiment. Except for these disagreements, the characteristic behavior of the energy dependence and the angular distribution is reasonably well reproduced within the wide energy range up to 800 MeV. These results indicate that the LS-RGM technique is very useful for investigating the baryon-baryon interaction above 300 MeV.

Figure 4 shows the five invariant amplitudes,  $g_0(\theta) \sim h_P(\theta)$ , as a function of the c.m. angle  $\theta$ , predicted by FSS for the  $np$  scattering at  $T_{lab} = 800$  MeV. The left column displays the real part, while the right column the imaginary part. The predictions by the Paris potential<sup>30)</sup> are also shown in the dashed curve for comparison. In these calculations the partial waves up to  $J = 8$  are included.\*) The

\*) Actually  $J_{max} = 8$  is not big enough for  $T_{lab} = 800$  MeV, as seen from the small ripples of the solid and dashed curves in Fig. 4. The partial-wave contributions for  $J > J_{max}$  from the Born

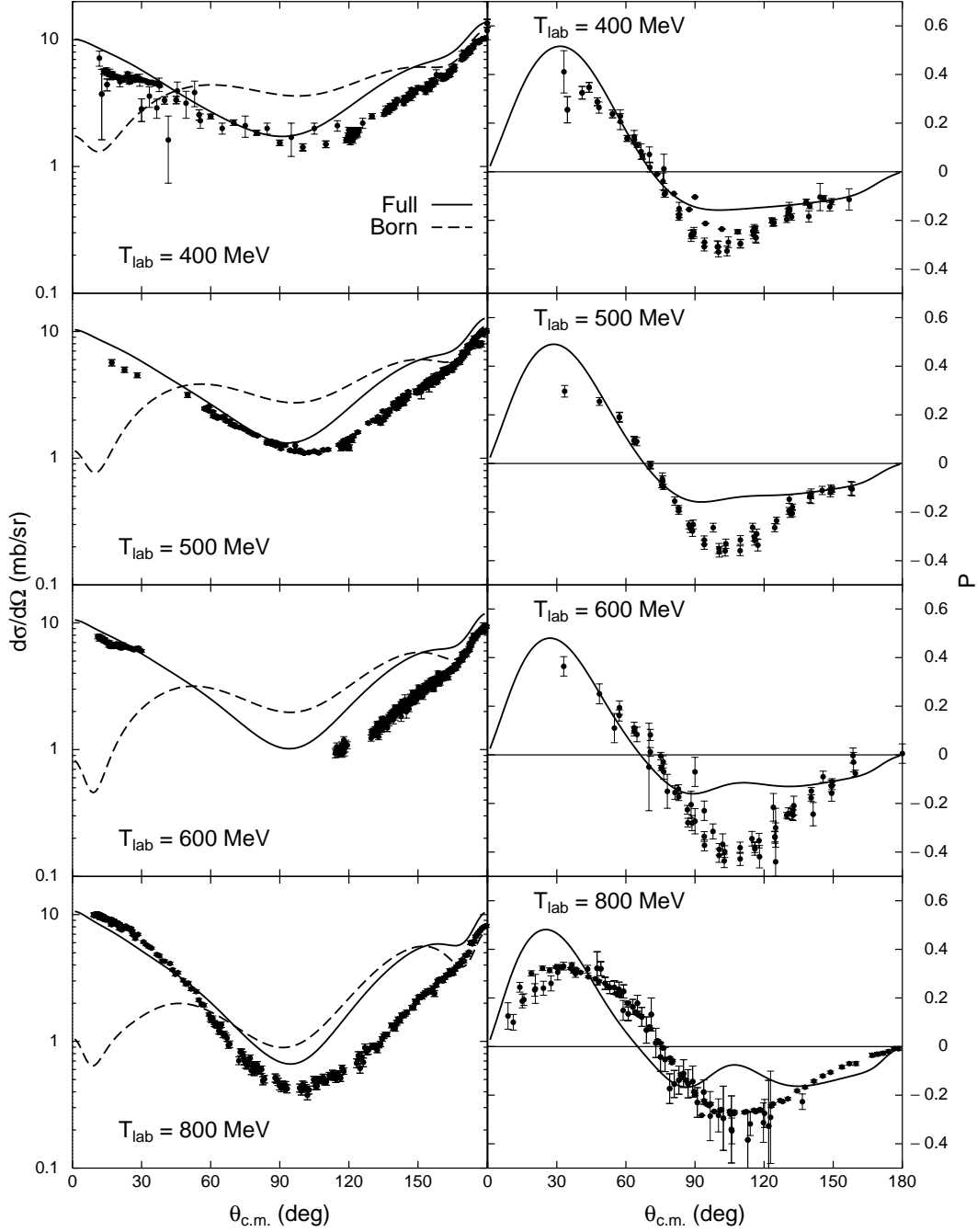


Fig. 2. The differential cross sections and polarization for the elastic  $np$  scattering at  $T_{lab} = 400 \sim 800$  MeV. The model is FSS. The solid curve denotes the full calculation with LS-RGM, while the dashed curve the one with the Born approximation. Experimental data are from 29).

amplitudes are added to obtain the results in Figs. 2 and 3.



dotted curve (Arndt) is the empirical value, which is calculated from the solution of the phase-shift analysis<sup>31)</sup> by using the real part of the phase-shift parameters up to  $J \leq 6$  and the partial-wave expansion of the invariant amplitudes Eq.(D.2). It

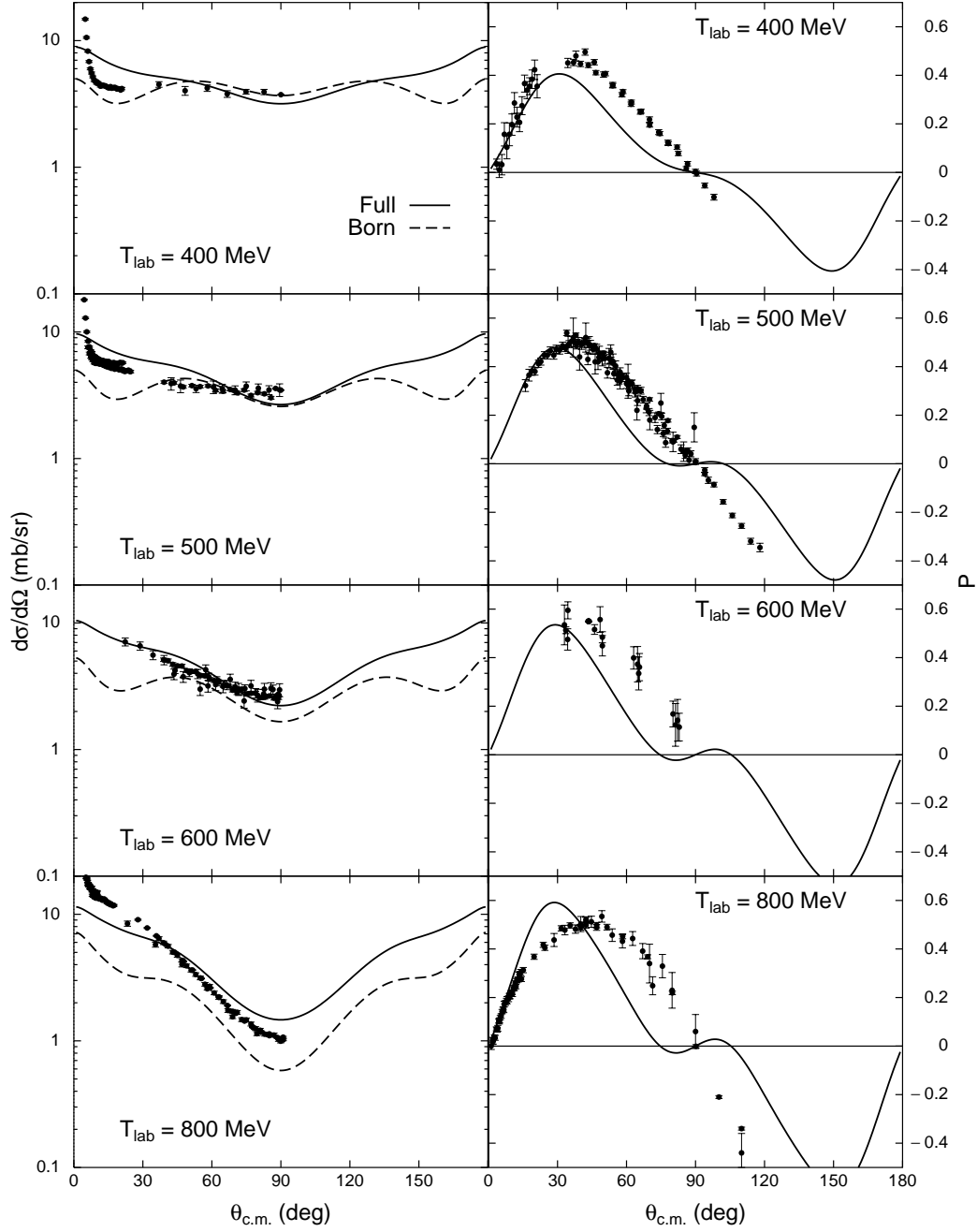


Fig. 3. The same as Fig. 2, but for the elastic  $pp$  scattering in model RGM-H. The Coulomb force is neglected.

is clear that the most prominent disagreement between the FSS prediction and the other predictions appears in the real part of the spin-independent central invariant amplitude  $\Re e g_0(\theta)$  at the forward angle. FSS predicts  $\Re e g_0(0) \sim 1.25$ , while the Paris potential and the phase-shift analysis predict  $\Re e g_0(0) \sim -1$ . If we use the  $t^{eff}\rho$  prescription discussed in § 2.4, these values correspond to the nucleon s.p. potential in normal nuclear matter,  $-17$  MeV for FSS and  $+14$  MeV for the latter two, as a

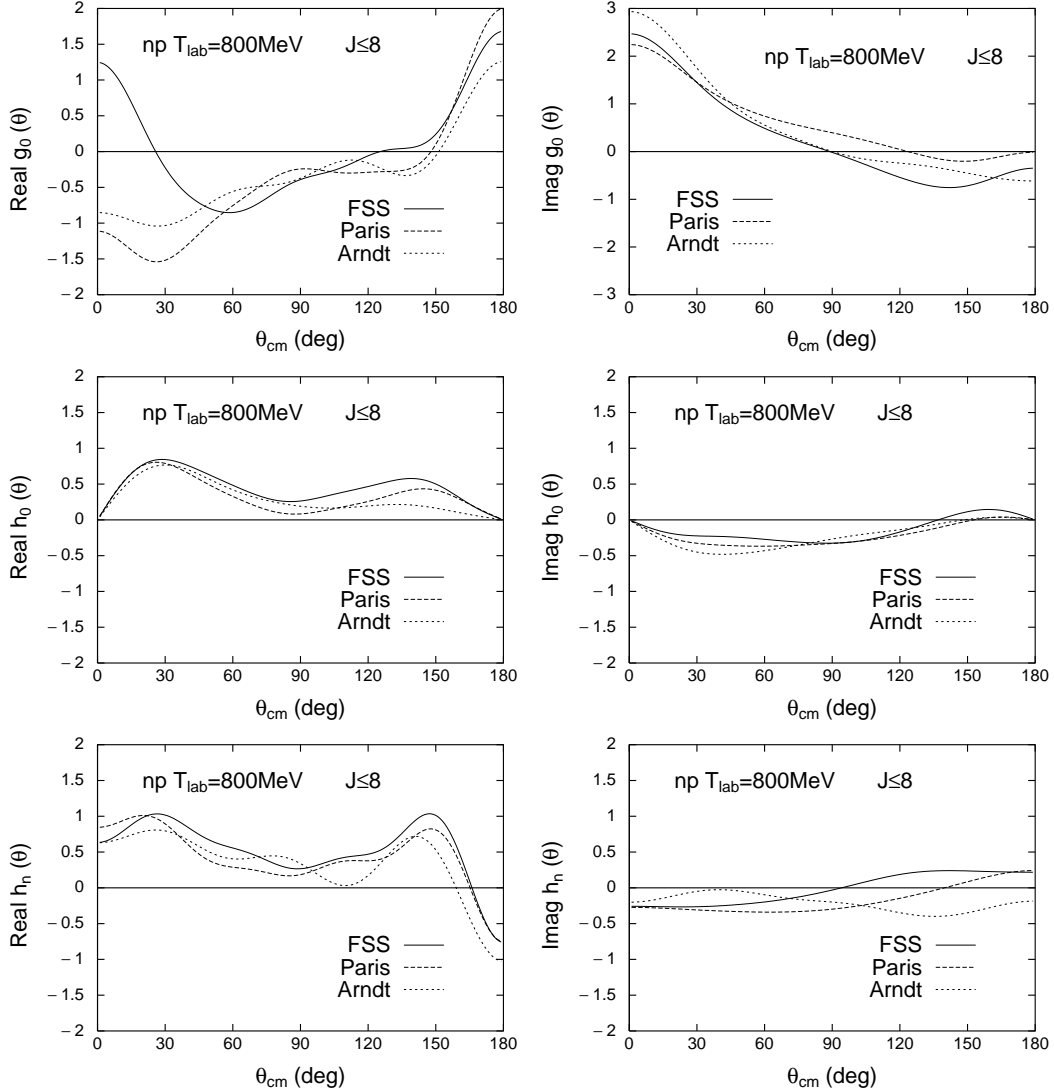


Fig. 4. The real (left) and imaginary (right) parts of the five invariant amplitudes,  $g_0(\theta) \sim h_P(\theta)$ , for the  $np$  elastic scattering at  $T_{lab} = 800$  MeV, predicted by model FSS. The dashed curve stands for predictions by the Paris potential<sup>30)</sup>, and the dotted curve those by the phase-shift analysis SP82 by Arndt *et al.*<sup>31)</sup>. The partial waves included are  $J \leq 6$  for SP82, and  $J \leq 8$  otherwise.

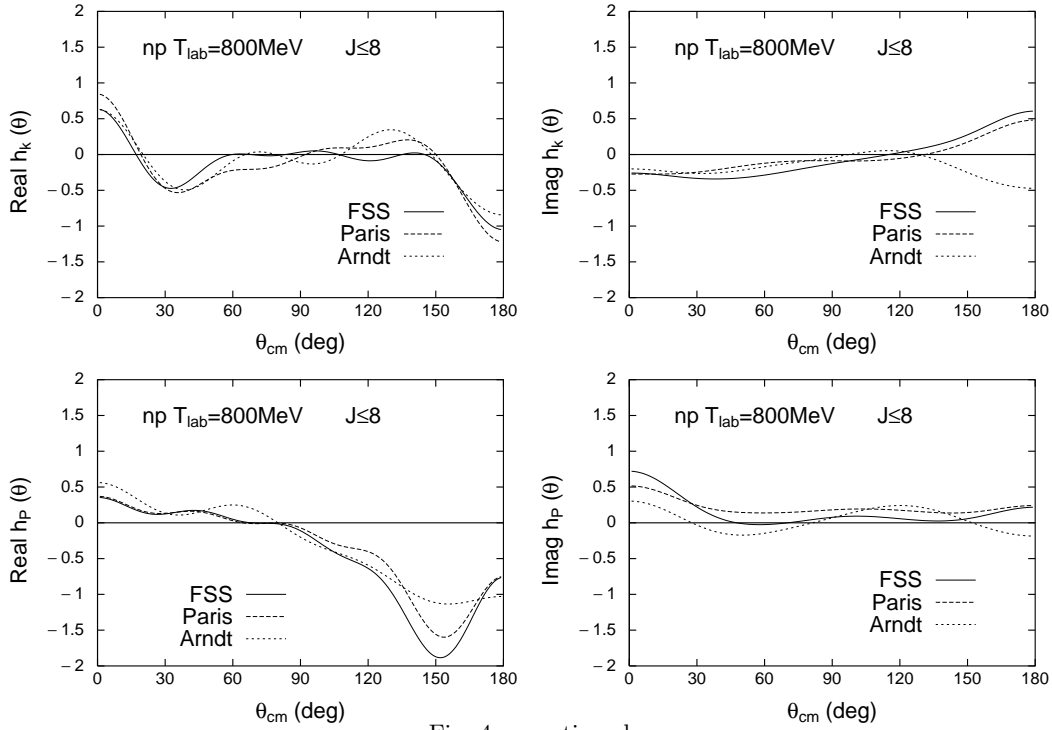


Fig. 4. -continued

contribution from the unlike nucleons.<sup>\*)</sup> We here find that the attractive behavior of the FSS s.p. potentials around this energy region is related to the wrong sign of the real part of the spin-independent central invariant amplitude  $\Re g_0(\theta)$  at the forward direction. This difference does not impair the differential cross sections very much, since the invariant amplitude has an appreciable magnitude for the imaginary part as seen in Fig. 4. This should, however, affect some particular polarization observables, and cause a large disagreement compared to experiment.

### §5. Nucleon and hyperon single-particle potentials in nuclear matter

Figure 5 illustrates s.p. potentials  $U_B(q_1)$ , as a function of the incident momentum  $q_1$ , which are obtained for  $B = N, \Lambda$  and  $\Sigma$  from the  $G$ -matrix calculations with the model FSS. The normal density with  $k_F = 1.35 \text{ fm}^{-1}$  is assumed for nuclear matter. The left panels are the results with  $QTQ$  prescription for intermediate energy spectra, while the right panels are those with the continuous prescription.<sup>15)</sup> The upper panels are for the momentum  $q_1 < 4 \text{ fm}^{-1}$ , while the lower panels for  $q_1 < 20 \text{ fm}^{-1}$ . In the  $QTQ$  prescription, the self-consistency of the s.p. potentials is not respected in the momentum region  $q_1 > k_F = 1.35 \text{ fm}^{-1}$ . On the other hand,

<sup>\*)</sup> These are consistent with the numbers given in Table VI. Namely, if we add up the  $I = 0$  contribution and one-third of the  $I = 1$  contribution to the real part of the s.p. potentials at 800 MeV, the potential depth becomes  $-17.4 \text{ MeV}$  for FSS,  $15.5 \text{ MeV}$  for the Paris potential, and  $14.5 \text{ MeV}$  for SP99.

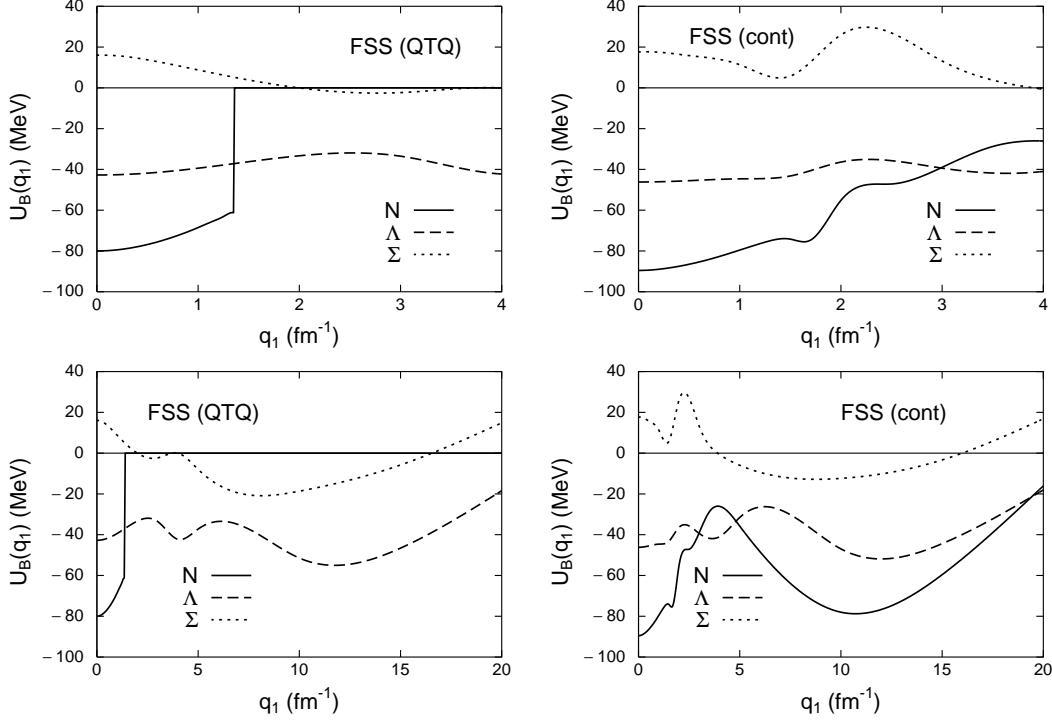


Fig. 5. The nucleon and hyperon ( $\Lambda$ ,  $\Sigma$ ) s.p. potentials predicted by the  $G$ -matrix calculation of model FSS. The results in the left panels are obtained by using  $QTQ$  prescription, while those in the right panels by the continuous prescription for intermediate energy spectra. The momentum interval is  $0 < q_1 < 4 \text{ fm}^{-1}$  in the upper panels, and  $0 < q_1 < 20 \text{ fm}^{-1}$  in the lower panels. The Fermi momentum  $k_F = 1.35 \text{ fm}^{-1}$  is assumed.

it is fully accounted for in the continuous prescription.<sup>\*)</sup> This implies that we first calculate  $U_N(q_1)$ , and then  $U_\Lambda(q_1)$  and  $U_\Sigma(q_1)$  are determined self-consistently by using the result of  $U_N(q_1)$ . The partial waves included are for  $J \leq 9$ . We can see from Fig. 5 that the s.p. potentials predicted by FSS is fairly strongly attractive in the momentum interval  $q_1 = 5 \sim 20 \text{ fm}^{-1}$  for all the baryons. In particular,  $U_N(q_1)$  in the continuous prescription becomes almost  $-80 \text{ MeV}$  at  $q_1 = 10 \text{ fm}^{-1}$ . This momentum interval corresponds to the incident energy  $T_{lab} = 500 \text{ MeV} \sim 8 \text{ GeV}$  in the  $NN$  scattering (see Table III). We therefore need to examine the invariant amplitudes carefully in this energy region.

Let us first examine whether the  $t^{eff\rho}$  prescription discussed in § 2.4 is a good approximation to the s.p. potentials predicted by the  $G$ -matrix calculation. Table III shows such a comparison with respect to the nucleon s.p. potential  $U_N(q_1)$  (in MeV) predicted by the model FSS. Here we find that the maximum value of the total angular momentum  $J_{max} = 7$  is actually too small, when the incident momentum

<sup>\*)</sup> In Ref. 15) we have assumed  $U_B(q_1) = U_B(q_1 = 3.8 \text{ fm}^{-1})$  for  $q_1 \geq 3.8 \text{ fm}^{-1}$ , in order to avoid the unrealistic behavior of the s.p. potentials in the high momentum region. Here  $q_1 = 3.8 \text{ fm}^{-1}$  corresponds to  $T_{lab} = 300 \text{ MeV}$  in the  $NN$  scattering.

Table III. Comparison of s.p. potential  $U_N(q_1)$  (in MeV), obtained by  $t^{eff}\rho$  prescription ( $T$ -matrix) and by  $G$ -matrix calculation in the continuous choice<sup>15)</sup>. The model is FSS<sup>5), 6)</sup>.

(Real part)

$T_{lab}$ (MeV)	$q_1$ (fm <sup>-1</sup> )	$T$ -matrix		$G$ -matrix (cont.)	
		$J \leq 9$	$J \leq 9$	$J \leq 9$	$J \leq 7$
187	3	-37.49	-37.49	-38.98	-36.76
332	4	-27.81	-27.81	-26.08	-23.75
518	5	-30.19	-30.19	-35.79	-33.01
2074	10	-79.90	-79.90	-78.00	-54.20
8295	20	-14.81	-14.81	-16.07	-7.82

(Imaginary part)

$T_{lab}$ (MeV)	$q_1$ (fm <sup>-1</sup> )	$T$ -matrix		$G$ -matrix (cont.)	
		$J \leq 9$	$J \leq 9$	$J \leq 9$	$J \leq 7$
187	3	-44.91	-44.91	-29.71	-29.53
332	4	-52.88	-52.88	-39.64	-39.43
518	5	-60.51	-60.51	-44.68	-44.88
2074	10	-34.91	-34.91	-36.81	-29.77
8295	20	-22.96	-22.96	-21.07	-2.92

Table IV. Decomposition of  $U_N(q_1)$  (in MeV) in Table III to the isospin  $I = 0$  and  $I = 1$  components. The total angular momentum included is  $J \leq 9$ . The model is FSS<sup>5), 6)</sup>.

(Real part)

$T_{lab}$ (MeV)	$q_1$ (fm <sup>-1</sup> )	$I = 0$		$I = 1$	
		$T$ -matrix	$G$ -matrix	$T$ -matrix	$G$ -matrix
187	3	-11.91	-15.25	-25.58	-23.73
332	4	-5.98	-7.53	-21.83	-18.55
518	5	-5.04	-9.65	-25.16	-26.14
2074	10	-28.72	-27.93	-51.18	-50.07
8295	20	-2.37	-3.60	-12.44	-12.47

(Imaginary part)

$T_{lab}$ (MeV)	$q_1$ (fm <sup>-1</sup> )	$I = 0$		$I = 1$	
		$T$ -matrix	$G$ -matrix	$T$ -matrix	$G$ -matrix
187	3	-22.02	-15.85	-22.89	-13.86
332	4	-22.66	-17.69	-30.22	-21.57
518	5	-22.21	-19.69	-38.30	-24.99
2074	10	-15.27	-14.83	-19.63	-21.99
8295	20	-20.62	-18.78	-2.34	-2.29

Table V. Reduction factors of the  $S$ -meson central attraction due to the momentum-dependent  $q^2$  term.

$q \sim k_{cm}$	$T_{lab}$	$0.0243 q^2$
2	332 MeV	0.097
3.1	800 MeV	0.23
5	2 GeV	0.61
7.5	4.7 GeV	1.37

$q_1 \geq 10 \text{ fm}^{-1}$ . However, if we take the same  $J_{max}$  in the two calculations, the accuracy of the  $t^{eff}\rho$  prescription seems to be fairly good even for the large momentum around  $q_1 \sim 10 \text{ fm}^{-1}$ . Quite surprisingly, this approximation is very good even at such a small energy as  $T_{lab} = 200 \text{ MeV}$ , as long as the real part of the s.p. potential is concerned. This agreement between the two prescriptions becomes clearer, if we examine each isospin component with  $I = 0$  and  $I = 1$ , separately, as seen from Table IV. As to the imaginary part of the s.p. potential, the  $t^{eff}\rho$  prescription seems to overestimate the values by the  $G$ -matrix calculation.

From this comparison and the behavior of the invariant amplitudes in the preceding section, we have found that the attractive behavior of  $U_N(q_1)$  in the momentum interval  $q_1 = 5 \sim 20 \text{ fm}^{-1}$  in FSS is related to the wrong sign (of the real part) of the spin-independent central invariant amplitude at the forward direction. We expect that this situation is common even for the  $\Lambda$  and  $\Sigma$  hyperons, and it is a flaw of our present quark model (not only FSS, but also RGM-H and RGM-F). It should be mentioned that the quantitative aspect of the present non-relativistic single-channel calculation in the above momentum region is not entirely trustable. The corresponding energy region of the  $NN$  scattering is already the relativistic energy region, where many inelastic channels are open. Nevertheless, a repulsive behavior of the s.p. potential at  $q_1 = 5 \sim 20 \text{ fm}^{-1}$  seems to be a mandatory requirement even in the single-channel calculation, since channel-coupling effects are expected to work attractive to the s.p. potential. Although this energy region may already be out of the applicability of our non-relativistic quark model, we need s.p. potentials for the intermediate states with quite high momenta when the  $G$ -matrix calculation is carried out in the continuous prescription.

In order to solve this problem, we use an advantage of our quark model that the effect of the short-range correlation is rather moderate compared with that of the standard meson-exchange potentials like the Paris potential. Namely, an improvement of the Born amplitudes is clearly reflected to the improvement of the solution of the LS-RGM equation. In particular, the intermediate-range attraction from the scalar-meson exchange has the Born kernel

$$V^C(\mathbf{k}, \mathbf{q}) = -\frac{g^2}{\mathbf{k}^2 + m^2} \left[ 1 - \frac{\mathbf{q}^2}{2M^2} + \frac{\mathbf{k}^2}{8M^2} \right] \quad (5.1)$$

with  $\mathbf{k} = \mathbf{q}_f - \mathbf{q}_i$  and  $\mathbf{q} = (\mathbf{q}_f + \mathbf{q}_i)/2$ , in the approximation up to the order of  $(v/c)^2$ . Here  $m$  and  $M$  are the meson mass and the baryon mass, respectively. So far we

have used only the leading term 1 in the square bracket of Eq. (5.1) and neglected  $\mathbf{q}^2$  and  $\mathbf{k}^2$  terms. A dominant contribution to the spin-independent central invariant amplitude at the forward angle comes from the  $\mathbf{q}^2$  term, which becomes important in the high-energy region. In fact, if we set  $\mathbf{k}^2 \rightarrow -m^2$  as usual, modify the square bracket of Eq. (5.1) as

$$\begin{aligned} & \left[ 1 - \frac{\mathbf{q}^2}{2M^2} + \frac{\mathbf{k}^2}{8M^2} \right] \longrightarrow \left[ 1 - \frac{\mathbf{q}^2}{2M^2} - \frac{m^2}{8M^2} \right] \\ & = \left( 1 - \frac{m^2}{8M^2} \right) \left[ 1 - \frac{1}{1 - m^2/8M^2} \frac{\mathbf{q}^2}{2M^2} \right], \end{aligned} \quad (5.2)$$

and redefine  $g^2$  including the  $(1 - m^2/8M^2)$  factor, we find the momentum dependence like  $1 - 0.0243 \mathbf{q}^2$  for the mass  $mc^2 = 800$  MeV of the  $\epsilon$  meson in FSS. Here  $|\mathbf{q}|$  is in units of  $\text{fm}^{-1}$ . This non-static term of the  $S$  mesons plays a role to reduce the strength of the intermediate-range attraction by about 20 % at 800 MeV. (See Table V.) Actually the momentum  $\mathbf{q}$  is not directly related to the total energy, nor the direct Born term is good enough to discuss the reduction of the central attraction at higher energies. We also have contributions from the inherent zero-point oscillation of the cluster wave functions and those from the quark-exchange kernel, since our EMEP are acting between quarks. Nevertheless, the discussion here is still valid, since the dominant contribution to the intermediate attraction is the direct term of the  $\epsilon$ -meson exchange potential. Bryan-Scott<sup>32)</sup> carefully examined these  $\mathbf{q}^2$  momentum-dependent terms in the S-meson and V-meson exchange potentials. They found that the inclusion of these terms has a favorable effect of making the non-relativistic approximation uniform to order  $\mathbf{q}^2$ , although the main effect is almost compensated for by a slight change in the coupling constants. Since these terms are included in the Paris potential<sup>30)</sup> and all the Nijmegen soft-core potentials<sup>33), 34)</sup>, it would be useful to incorporate these terms in our quark model, in order to describe correctly the asymptotic behavior of the s.p. potentials in the high-momentum region.

As an example of the quark model with the momentum-dependent  $\mathbf{q}^2$  term, we show in Table VI the result of the s.p. potential  $U_N(q_1)$  in the  $t^{eff}\rho$  prescription, calculated by a new model (present). In this new model V-mesons are also incorporated as the EMEP acting between quarks. The phase-shift parameters of the  $np$  scattering is largely improved in comparison with those of FSS. The details of this new model will be published elsewhere. In Table VI predictions of the Paris potential<sup>30)</sup> and of the phase-shift analysis SP99<sup>29)</sup>, together with the decomposition to  $I = 0$  and  $I = 1$  contributions, are also shown for comparison. We find that the new model is still slightly too attractive around  $T_{lab} \sim 800$  MeV, but the flaw of FSS with too attractive asymptotic behavior in the high-momentum region is clearly removed.

## §6. Summary

In the quark-model study of the nucleon-nucleon ( $NN$ ) and hyperon-nucleon ( $YN$ ) interactions, a variational method is usually used to solve an integro-differ-

Table VI. Comparison of  $U_N(q_1)$  (in MeV) in the  $t^{eff}\rho$  prescription and its decomposition to the isospin  $I = 0$  and  $I = 1$  components, with other models (Paris<sup>30</sup>) and experiment (SP99<sup>29</sup>). The result by a new model with the momentum-dependent  $\mathbf{q}^2$  term (present) is also shown.

$T_{lab}$ (MeV) or $q_1$ (fm <sup>-1</sup> )	FSS ( $J \leq 8$ )					
	$I = 0$		$I = 1$		total	
	real	imag	real	imag	real	imag
200	-11.43	-22.08	-25.47	-23.48	-36.90	-45.56
400	-5.11	-22.59	-23.81	-33.51	-28.92	-56.11
800	-5.58	-19.64	-35.41	-44.37	-40.99	-64.01
$q_1=10$	-17.36	-10.48	-53.92	-19.57	-71.27	-30.05
$q_1=20$	-7.04	-1.83	-12.52	-2.34	-19.56	-4.16
$T_{lab}$ (MeV) or $q_1$ (fm <sup>-1</sup> )	present ( $J \leq 8$ )					
	$I = 0$		$I = 1$		total	
	real	imag	real	imag	real	imag
200	-9.40	-16.72	-26.02	-20.72	-35.42	-37.45
400	-1.90	-16.11	-13.41	-26.58	-15.31	-42.70
800	4.18	-15.48	-4.24	-38.18	-0.06	-53.63
$q_1=10$	13.44	-11.52	29.23	-50.58	42.67	-62.10
$q_1=20$	39.4	-47.3	176	-150	215	-197
$T_{lab}$ (MeV) or $q_1$ (fm <sup>-1</sup> )	Paris potential ( $J \leq 8$ )					
	$I = 0$		$I = 1$		total	
	real	imag	real	imag	real	imag
200	-9.23	-17.74	-27.37	-19.50	-36.60	-37.25
400	0.65	-16.87	-10.76	-25.09	-10.11	-41.96
800	10.28	-18.97	15.68	-36.98	25.96	-55.95
$q_1=10$	25.67	-34.83	78.49	-89.93	104	-125
$q_1=20$	32.78	-83.78	143	-266	176	-350
$T_{lab}$ (MeV)	SP99 (Phase shift analysis) ( $J \leq 7$ )					
	$I = 0$		$I = 1$		total	
	real	imag	real	imag	real	imag
200	-8.56	-16.37	-25.68	-19.76	-34.24	-36.13
400	3.12	-15.08	-15.87	-30.13	-12.76	-45.21
800	13.28	-16.51	3.53	-74.20	16.82	-90.71

ential equation formulated in the  $(3q)$ - $(3q)$  resonating-group method (RGM). In this paper we have developed a Lippmann-Schwinger formalism for the  $(3q)$ - $(3q)$  RGM as an alternative method to the improved variational method<sup>11</sup>). The basic equation, which we call the LS-RGM equation, is completely equivalent to the standard RGM equation in the coordinate representation on the energy-shell. An advantage of solving the RGM equation in the momentum representation is to avoid rapid oscillation of the relative wave functions at higher energies, which leads to the strong cancellation of Gaussian trial functions in the improved variational method. This



feature of the LS-RGM formalism naturally makes it possible to obtain an accurate  $S$ -matrix even for the relativistic energies  $T_{lab} \geq 350$  MeV, where many inelastic channels open. Since the  $S$ -matrix is very accurate also in the low-energy region, an extension to the coupled-channel systems with different threshold energies is very successful.

In this formulation the Born kernel is analytically calculated for all pieces of direct and exchange terms, which are composed of the kinetic-energy term and various pieces of quark-quark ( $qq$ ) interactions. The  $qq$  interactions are further divided into the phenomenological confinement potential, a color analogue of the Fermi-Breit (FB) interaction, and the effective meson-exchange potentials (EMEP) acting between quarks. The Born kernel is then decomposed into partial-wave components and the resultant LS-RGM equation is solved by using the techniques developed by Noyes<sup>13)</sup> and Kowalski<sup>14)</sup>. Since calculations are always carried out in the momentum representation, the present formalism has no difficulty to incorporate the momentum-dependent  $qq$  interaction such as the momentum-dependent Breit retardation term of the FB interaction, the higher-order terms of the central scalar-meson and vector-meson exchange potentials, and the quadratic  $LS$  force. A convenient transformation formula to derive spatial functions for the direct and exchange kernels is given for a very general type of two-body interactions. The numerical evaluation of the partial-wave Born kernel is also best suited to convert the LS-RGM equation to the  $G$ -matrix (Bethe-Goldstone) equation<sup>15)</sup>, in which the Pauli principle is treated exactly at the baryon level.

The accuracy of the LS-RGM formalism has been examined in the  $\Lambda N$ - $\Sigma N$  ( $I = 1/2$ ) coupled-channel system. In this system the  ${}^3S_1$ - ${}^3D_1$  coupling caused by the very strong one-pion tensor force yields a prominent cusp structure for the  $\Lambda N$  phase-shift parameters at the  $\Sigma N$  threshold. On the other hand, a resonance appears either in  $\Lambda N$   ${}^1P_1$  state or in  $\Sigma N$   ${}^3P_1$  state by the strong effect of the antisymmetric  $LS$  force ( $LS^{(-)}$  force) originating from the FB interaction. The behavior of these resonances is rather sensitive to the characteristics of the model, particularly to the strength of the central attraction of the  $\Sigma N$  ( $I = 1/2$ ) channel. We have examined the model RGM-F and obtained a satisfactory agreement of the phase-shift parameters between the LS-RGM method and the improved variational method, in the wide momentum region  $p_{lab} = 0 \sim 1$  GeV/ $c$ .

Using the same parameter set determined at  $T_{lab} = 0 \sim 250$  MeV, we have extended our calculation of the differential cross sections and the polarization for the  $NN$  scattering to the intermediate energies  $T_{lab} = 400 \sim 800$  MeV. Although agreement with the experimental data becomes gradually worse as the energy becomes higher, the characteristic behavior of the energy dependence and the angular distribution of these observables for the elastic  $np$  and  $pp$  scattering are reasonably reproduced within this energy range. In particular, the invariant amplitudes predicted by model FSS for the  $np$  scattering at  $T_{lab} = 800$  MeV reproduce reasonably well the empirical invariant amplitudes determined from the phase shift analysis, except for a few typical disagreements. The most prominent disagreement appears in the real part of the spin-independent central invariant amplitude  $g_0(\theta)$  at the forward angles  $\theta \sim 0$ . This amplitude is related to the single-particle (s.p.) potential obtained from

the  $G$ -matrix calculation through the  $t^{eff}\rho$  prescription, when the incident momentum is high. The wrong sign of  $\Re g_0(\theta)$  at  $\theta = 0$  in our model is correlated to too attractive s.p. potentials in the momentum region  $q_1 = 5 \sim 20 \text{ fm}^{-1}$ .

We have also examined the accuracy of the  $t^{eff}\rho$  prescription by using the  $G$ -matrix solution<sup>15)</sup> and the present LS-RGM formalism. This prescription is a good approximation for the real part of the s.p. potentials in the energy region from  $T_{lab} = 200 \text{ MeV}$  to several GeV ( $q_1 = 3 \text{ fm}^{-1} \sim 20 \text{ fm}^{-1}$ ), as long as the maximum value of the angular-momentum cut for partial waves is commonly taken. On the other hand, the imaginary parts of the s.p. potentials are usually overestimated in the  $t^{eff}\rho$  prescription.

Perhaps the most striking feature of the quark model found in this investigation is a moderate effect of the short-range correlation. In the standard meson-exchange models, the observed phase-shifts are reproduced as a cancellation of very strong repulsive and attractive local potentials, and the Born amplitudes of the Paris potential, for example, are one or two order of magnitude large, compared to the empirical invariant amplitudes. On the other hand, the short-range repulsion in the quark model originates mainly from the nonlocal kernel of the color-magnetic term of the FB interaction. Born amplitudes of the quark model therefore have almost the same order of magnitude as the empirical amplitudes obtained by solving the LS-RGM equation. This implies that the short-range correlation in the quark model is rather moderate compared with the meson-exchange models. It can also be seen in our recent quark-model study of the s.p. spin-orbit potentials for the nucleon and hyperons. In Ref. 35) we have calculated the strength factor,  $S_B$ , of the s.p. spin-orbit potentials by using the  $G$ -matrix solutions and found that  $S_N$  does not obtain much effect of the short-range correlation, on the contrary to the standard potential models like the Reid soft-core potential with the strong short-range repulsive core. Since the Born amplitudes in the quark model reflect rather faithfully characteristics of the LS-RGM solution, it is easy to find missing ingredients that impair the model. In fact, we have discussed that the wrong sign of the invariant amplitude  $\Re g_0(\theta)$  in our quark model is related to our neglect of higher-order momentum-dependent central term of the scalar-meson exchange EMEP. A preliminary result of a new model, which incorporates this term as well as the vector-meson EMEP, shows that the s.p. potentials in the  $t^{eff}\rho$  prescription have a correct repulsive behavior in the asymptotic momentum region. The details of this model will be given in a forthcoming paper.

## Appendix A

— *A transformation formula to the Born kernel for momentum-dependent two-body interactions* —

As to the general procedure how to calculate the RGM kernel for two-cluster systems composed of  $s$ -shell clusters, Refs. 22) and 23) should be referred to. Here we use the same notation as Ref. 23) and give a convenient formula to calculate the Born kernel for two-body interactions with momentum dependence.

Suppose a two-body interaction of the RGM Hamiltonian is given by  $v_{ij} = u_{ij}w_{ij}$

with the spatial part  $u = u(\mathbf{r}, \partial/\partial\mathbf{r})$  and the spin-flavor-color part  $w_{ij} = w_{ij}^{SF} w_{ij}^C$ . The full Born kernel for this interaction is defined by

$$\langle e^{i\mathbf{q}_f \cdot \mathbf{r}} \phi | \sum_{i < j}^6 v_{ij} \mathcal{A}' | e^{i\mathbf{q}_i \cdot \mathbf{r}} \phi \rangle , \quad (\text{A}\cdot 1)$$

where  $\phi = \phi^{space} \xi$  with  $\xi = \xi^{SF} \xi^C$  is the harmonic-oscillator (h.o.) internal wave function of the  $(3q)$ - $(3q)$  system and  $\mathcal{A}'$  is the antisymmetrization operator between two clusters. This expression is reduced to the form Eq. (2.14) by the use of the double coset expansion  $\mathcal{A}' \rightarrow (1/2)(1 - 9P_{36})(1 - P_0)$  with  $P_0 = P_{14}P_{25}P_{36}$ , yielding the basic Born kernel Eqs. (2.22) and (2.25) with

$$M(\mathbf{q}_f, \mathbf{q}_i) = \sum_{x\mathcal{T}} X_{x\mathcal{T}} M_{x\mathcal{T}}(\mathbf{q}_f, \mathbf{q}_i) . \quad (\text{A}\cdot 2)$$

Here the superscript  $\Omega$  for specifying the type of the interaction is omitted for simplicity, and the sum over  $x$  is only for  $x = 0$  and 1. Furthermore,  $X_{x\mathcal{T}}$  is the spin-flavor-color factor defined through

$$\begin{aligned} X_{x\mathcal{T}} &= C_x \langle z_x \xi | \sum_{i < j}^{\mathcal{T}} w_{ij} | \xi \rangle \\ &= \begin{cases} X_{0\mathcal{T}}^C \langle \xi^{SF} | \sum_{i < j}^{\mathcal{T}} w_{ij}^{SF} | \xi^{SF} \rangle \\ (-9)X_{1\mathcal{T}}^C \langle P_{36} \xi^{SF} | \sum_{i < j}^{\mathcal{T}} w_{ij}^{SF} | \xi^{SF} \rangle \end{cases} \quad \text{for } x = \begin{cases} 0 \\ 1 \end{cases} , \quad (\text{A}\cdot 3) \end{aligned}$$

where  $x = 0$  with  $z_0 = 1$  and  $C_0 = 1$  corresponds to the direct term and  $x = 1$  with  $z_1 = P_{36}$  and  $C_1 = -9$  the (one-quark) exchange term. The suffix  $\mathcal{T}$  stands for the interaction type  $\mathcal{T} = E, S, S', D_+$  or  $D_-$ , for which the  $(i, j)$  pairs are properly selected. The color-factors  $X_{x\mathcal{T}}^C = \langle z_x \xi^C | w_{ij}^C | \xi^C \rangle$  for each  $(i, j) \in \mathcal{T}$  are given as follows. For the quark sector with  $w_{ij}^C = (1/4)(\lambda_i^C \lambda_j^C)$ ,  $X_{0E}^C = -(2/3)$ ,  $X_{0D_+}^C = 0$ , and  $X_{1E}^C = X_{0S}^C = X_{0S'}^C = -(2/9)$ ,  $X_{1D_+}^C = 1/9$ ,  $X_{1D_-}^C = 4/9$ . For the EMEP sector with  $w_{ij}^C = 1$ ,  $X_{0\mathcal{T}}^C = 1$  and  $X_{1\mathcal{T}}^C = 1/3$ . The spin-flavor-color factor for the exchange normalization kernel is defined by  $X_N = (-3)\langle P_{36} \xi^{SF} | \xi^{SF} \rangle$ . We also need  $X_K = 24\langle P_{36} \xi^{SF} | Y(6) - Y(5) | \xi^{SF} \rangle$  for the exchange kinetic-energy kernel of the  $YN$  systems. On the other hand, the spatial part of the Born kernel is defined by

$$M_{x\mathcal{T}}(\mathbf{q}_f, \mathbf{q}_i) = \langle z_x e^{i\mathbf{q}_f \cdot \mathbf{r}} \phi^{space} | u_{ij} | e^{i\mathbf{q}_i \cdot \mathbf{r}} \phi^{space} \rangle \quad \text{with } (i, j) \in \mathcal{T} , \quad (\text{A}\cdot 4)$$

which we now evaluate.

The standard procedure is to use the h.o. generating function

$$A_\gamma(\mathbf{r}, \mathbf{z}) = \left( \frac{2\gamma}{\pi} \right)^{\frac{3}{4}} e^{-\gamma(\mathbf{r} - \mathbf{z}/\sqrt{\gamma})^2 + \mathbf{z}^2/2} , \quad (\text{A}\cdot 5)$$

and first to calculate the so-called complex GCM kernel defined by

$$I_{x\mathcal{T}}(\mathbf{z}, \mathbf{z}') = \langle z_x A_\gamma(\mathbf{r}, \mathbf{z}) \phi^{space} | u_{ij} | A_\gamma(\mathbf{r}, \mathbf{z}') \phi^{space} \rangle . \quad (\text{A}\cdot 6)$$

This GCM kernel is divided into the general form of the norm kernel and the interaction function  $\mathcal{T}(\mathbf{z}, \mathbf{z}')$ :

$$\begin{aligned} I_x \mathcal{T}(\mathbf{z}, \mathbf{z}') &= e^{(1-\frac{x}{\mu})\mathbf{z}\cdot\mathbf{z}'} \mathcal{T}(\mathbf{z}, \mathbf{z}') \quad , \\ \mathcal{T}(\mathbf{z}, \mathbf{z}') &= \langle (0s)_{\mathbf{S}_\alpha} | (0s)_{\mathbf{S}'_\beta} \rangle^{-1} \langle (0s)_{\mathbf{S}_\gamma} | (0s)_{\mathbf{S}'_\delta} \rangle^{-1} \\ &\quad \times \langle (0s)_{\mathbf{S}_\alpha} (0s)_{\mathbf{S}_\gamma} | u | (0s)_{\mathbf{S}'_\beta} (0s)_{\mathbf{S}'_\delta} \rangle \quad . \end{aligned} \quad (\text{A}\cdot 7)$$

Here  $(0s)_{\mathbf{S}}$  stands for a localized  $(0s)$  wave function around  $\mathbf{x} = \mathbf{S}$ , and  $\mathbf{S}_\alpha$  etc. are the generator coordinates specifying the position of clusters<sup>23)</sup>. For a simple Gaussian two-body interaction  $u(\mathbf{r}) \sim e^{-\kappa r^2}$ ,  $\mathcal{T}(\mathbf{z}, \mathbf{z}')$  is given by

$$\mathcal{T}(\mathbf{z}, \mathbf{z}') = \left( \frac{\nu}{\nu + \kappa} \right)^{\frac{3}{2}} e^{-\frac{\lambda}{2}(p\mathbf{z}^* + q\mathbf{z}')^2} \times (\text{polynomial terms}) \quad , \quad (\text{A}\cdot 8)$$

where  $\nu = 1/2b^2$  is the h.o. constant of the  $(0s)$  clusters and  $\lambda$  is given by  $\lambda = (1/2\mu)(\kappa/(\nu + \kappa))$  with  $\gamma = \mu\nu$  and  $\mu = 3 \cdot 3/(3+3) = 3/2$ . The parameters  $p$  and  $q$  are 0, 1 or  $-1$ , depending on  $\mathcal{T}$ , which are explicitly given in TABLE II of Ref. 23). The transformation to the Born kernel is achieved through

$$\begin{aligned} M_{x\mathcal{T}}(\mathbf{q}_f, \mathbf{q}_i) &= \left( \frac{\gamma}{2\pi} \right)^{\frac{3}{2}} e^{\frac{1}{4\gamma}(\mathbf{q}_f^2 + \mathbf{q}_i^2)} \int d\mathbf{a} d\mathbf{b} e^{-\frac{\gamma}{2}(\mathbf{a}^2 + \mathbf{b}^2)} e^{-i\mathbf{q}_f \cdot \mathbf{a} + i\mathbf{q}_i \cdot \mathbf{b}} \\ &\quad \times I_{x\mathcal{T}}(\sqrt{\gamma}\mathbf{a}, \sqrt{\gamma}\mathbf{b}) \quad . \end{aligned} \quad (\text{A}\cdot 9)$$

When  $u$  involves momentum-dependence, it is convenient to use the momentum representation and write

$$\langle \mathbf{p} | u | \mathbf{p}' \rangle = \frac{1}{(2\pi)^3} u(\mathbf{k}', \mathbf{q}') \quad \text{with} \quad \mathbf{k}' = \mathbf{p} - \mathbf{p}', \quad \mathbf{q}' = \frac{1}{2}(\mathbf{p} + \mathbf{p}') \quad . \quad (\text{A}\cdot 10)$$

Then the interaction function in Eq. (A·7) is given by

$$\begin{aligned} \mathcal{T}(\mathbf{z}, \mathbf{z}') &= \frac{1}{(2\pi)^3} \left( \frac{1}{\pi\nu} \right)^{\frac{3}{2}} \int d\mathbf{k}' d\mathbf{q}' e^{-\frac{1}{\nu}(\mathbf{q}'^2 + \frac{1}{4}\mathbf{k}'^2)} e^{\frac{1}{4}\nu r^2 + i\mathbf{q}' \cdot \mathbf{r}} e^{i\mathbf{k}' \cdot \mathbf{X}} u(\mathbf{k}', \mathbf{q}') \\ &\quad \text{with} \quad \mathbf{r} = -\frac{1}{\sqrt{\gamma}}(p\mathbf{z}^* - q\mathbf{z}'), \quad \mathbf{X} = -\frac{1}{2\sqrt{\gamma}}(p\mathbf{z}^* + q\mathbf{z}') \quad . \end{aligned} \quad (\text{A}\cdot 11)$$

If we use Eq. (A·11) in Eq. (A·9), the integration over  $\mathbf{a}$  and  $\mathbf{b}$  can be carried out and we obtain the following formula after some rearrangement of terms:

$$\begin{aligned} M_{x\mathcal{T}}(\mathbf{q}_f, \mathbf{q}_i) &= M_x^N(\mathbf{q}_f, \mathbf{q}_i) \left( \frac{1}{2\pi} \right)^3 \int d\mathbf{k}' \exp \left\{ - \left( 1 + \frac{\tilde{\alpha}}{2\mu} \right) \frac{1}{4\nu} \mathbf{k}'^2 - \frac{1}{2\sqrt{\gamma}} \mathbf{V} \mathbf{k}' \right\} \\ &\quad \times \left( \frac{1}{\pi\nu} \frac{1}{1 - \alpha/2\mu} \right)^{3/2} \int d\mathbf{q}' \exp \left\{ - \frac{1}{\nu} \frac{1}{1 - \alpha/2\mu} \mathbf{q}'^2 \right\} \\ &\quad \times u \left( \mathbf{k}', \mathbf{q}' - \frac{\varepsilon}{4\mu} \mathbf{k}' - \frac{\nu}{2\sqrt{\gamma}} \mathbf{A} \right) \quad . \end{aligned} \quad (\text{A}\cdot 12)$$

Here  $M_x^N(\mathbf{q}_f, \mathbf{q}_i)$  is the normalization kernel given by

$$M_x^N(\mathbf{q}_f, \mathbf{q}_i) = \left( \frac{2\pi}{\gamma} \frac{1}{1-\tau^2} \right)^{3/2} \exp \left\{ -\frac{1}{2\gamma} \left( \frac{1-\tau}{1+\tau} \mathbf{q}^2 + \frac{1+\tau}{1-\tau} \frac{1}{4} \mathbf{k}^2 \right) \right\}, \quad (\text{A}\cdot 13)$$

with  $\tau = 1 - x/\mu$ ,  $\mathbf{k} = \mathbf{q}_f - \mathbf{q}_i$  and  $\mathbf{q} = (\mathbf{q}_f + \mathbf{q}_i)/2$ , and the coefficients appearing in Eq. (A.12) are defined by

$$\begin{aligned} \alpha &= \frac{p^2 + q^2 - 2\tau pq}{1 - \tau^2}, \quad \tilde{\alpha} = \frac{p^2 + q^2 + 2\tau pq}{1 - \tau^2}, \quad \varepsilon = \frac{p^2 - q^2}{1 - \tau^2}, \\ \mathbf{V} &= \frac{1}{\sqrt{\gamma}} \left( \frac{p-q}{1+\tau} \mathbf{q} + \frac{p+q}{1-\tau} \frac{1}{2} \mathbf{k} \right), \quad \mathbf{A} = \frac{1}{\sqrt{\gamma}} \left( \frac{p+q}{1+\tau} \mathbf{q} + \frac{p-q}{1-\tau} \frac{1}{2} \mathbf{k} \right). \end{aligned} \quad (\text{A}\cdot 14)$$

Let us specialize the two-body interaction to the Yukawa function and the Gaussian function:

$$u(\mathbf{k}, \mathbf{q}) = \begin{cases} \frac{4\pi}{\mathbf{k}^2 + m^2} \tilde{u}(\mathbf{k}, \mathbf{q}) \\ \left( \frac{\pi}{\kappa} \right)^{\frac{3}{2}} e^{-\frac{1}{4\kappa} \mathbf{k}^2} \tilde{u}(\mathbf{k}, \mathbf{q}) \end{cases}. \quad (\text{A}\cdot 15)$$

Here  $\tilde{u}(\mathbf{k}, \mathbf{q})$  stands for a polynomial function of  $\mathbf{k}$  and  $\mathbf{q}$ , and the degree of the polynomial is usually at most the second order in  $\mathbf{q}$ . The Born kernel for the Yukawa function is calculated from the formula for the Gaussian function through the integral representation

$$\frac{4\pi}{\mathbf{k}^2 + m^2} = m \frac{1}{\sqrt{\pi}} \int_0^\infty du e^{-\frac{1}{u^2}} \left( \frac{\pi}{\kappa} \right)^{\frac{3}{2}} e^{-\frac{1}{4\kappa} \mathbf{k}^2} \quad \text{with} \quad \kappa = \left( \frac{mu}{2} \right)^2. \quad (\text{A}\cdot 16)$$

The resultant Born kernel is expressed by generalized Dawson's integrals  $\tilde{h}_n(x)$  and modified Yukawa functions  $\tilde{\mathcal{Y}}_\alpha(x)$ ,  $\tilde{\mathcal{Z}}_\alpha(x)$  etc., which are given by the error function of the imaginary argument:

$$\begin{aligned} \tilde{h}_n(x) &= (2n+1) e^{-x^2} \int_0^1 e^{x^2 t^2} t^{2n} dt = (2n+1) \frac{e^{-x^2}}{x^{2n+1}} \int_0^x e^{u^2} u^{2n} du, \\ \tilde{\mathcal{Y}}_\alpha(x) &= e^{\alpha-x^2} \int_0^1 e^{-\frac{\alpha}{t^2} + x^2 t^2} dt, \\ \tilde{\mathcal{Z}}_\alpha(x) &= e^{\alpha-x^2} \int_0^1 e^{-\frac{\alpha}{t^2} + x^2 t^2} t^4 dt. \end{aligned} \quad (\text{A}\cdot 17)$$

For the Gaussian kernel Eq. (A.12) is reduced into

$$M_{x\mathcal{T}}(\mathbf{q}_f, \mathbf{q}_i) = M_x^N(\mathbf{q}_f, \mathbf{q}_i) \left( \frac{\nu}{\nu + \kappa} \frac{1}{1 + \lambda \tilde{\alpha}} \right)^{\frac{3}{2}} \exp \left\{ \frac{1}{2} \frac{\lambda}{1 + \lambda \tilde{\alpha}} \mathbf{V}^2 \right\} \mathcal{P}(\mathbf{q}_f, \mathbf{q}_i), \quad (\text{A}\cdot 18)$$

where the polynomial part is given by

$$\mathcal{P}(\mathbf{q}_f, \mathbf{q}_i) = \left( \frac{1 + \lambda \tilde{\alpha}}{8\pi\gamma\lambda} \right)^{\frac{3}{2}} \int \mathbf{k}' \exp \left\{ -\frac{1 + \lambda \tilde{\alpha}}{8\gamma\lambda} \mathbf{k}'^2 \right\}$$

$$\begin{aligned} & \times \left( \frac{1}{\pi\nu} \frac{1}{1 - \alpha/2\mu} \right)^{3/2} \int d\mathbf{q}' \exp \left\{ -\frac{1}{\nu} \frac{1}{1 - \alpha/2\mu} \mathbf{q}'^2 \right\} \\ & \times \tilde{u} \left( \mathbf{k}' + 2\sqrt{\gamma}\tilde{\mathbf{V}}, \mathbf{q}' - \frac{\varepsilon}{4\mu}\mathbf{k}' + \frac{\nu}{2\sqrt{\gamma}}\mathbf{W} \right) . \end{aligned} \quad (\text{A}\cdot 19)$$

Here  $\tilde{u}(\mathbf{k}', \mathbf{q}') = \tilde{u}(-\mathbf{k}', -\mathbf{q}')$  and the simplified notation

$$\tilde{\mathbf{V}} = \frac{\lambda}{1 + \lambda\tilde{\alpha}} \mathbf{V} \quad , \quad \mathbf{W} = \mathbf{A} - \varepsilon\tilde{\mathbf{V}} \quad (\text{A}\cdot 20)$$

are used. If  $u(\mathbf{k}, \mathbf{q})$  does not involve  $\mathbf{q}$ -dependence, the  $\mathbf{q}'$  integral is carried out in Eq. (A.19) and we obtain

$$\mathcal{P}(\mathbf{q}_f, \mathbf{q}_i) = \left( \frac{1 + \lambda\tilde{\alpha}}{8\pi\gamma\lambda} \right)^{\frac{3}{2}} \int \mathbf{k}' \exp \left\{ -\frac{1 + \lambda\tilde{\alpha}}{8\gamma\lambda} \mathbf{k}'^2 \right\} \tilde{u} \left( \mathbf{k}' + 2\sqrt{\gamma}\tilde{\mathbf{V}} \right) . \quad (\text{A}\cdot 21)$$

## Appendix B

### — Born kernel —

In this appendix we show the invariant Born kernel Eq. (2.25) obtained by using the transformation formula in Appendix A. These are functions of  $\mathbf{k}^2$ ,  $\mathbf{q}^2$  and  $\mathbf{k} \cdot \mathbf{q}$  with  $\mathbf{k} = \mathbf{q}_f - \mathbf{q}_i$ ,  $\mathbf{q} = (\mathbf{q}_f + \mathbf{q}_i)/2$ , and expressed by the special functions given in Eq. (A.17). Only  $\theta$  with  $\cos \theta = \hat{\mathbf{q}}_f \cdot \hat{\mathbf{q}}_i$  is explicitly written in the spatial functions  $f_{\mathcal{T}}^{\mathcal{Q}}(\theta)$ . The  $S'$ -type spatial function  $f_{S'}^{\mathcal{Q}}(\theta)$  is obtained from  $f_S^{\mathcal{Q}}(\theta)$  with  $\mathbf{k} \rightarrow -\mathbf{k}$ . There is no  $E$ -type possible for the non-central forces. The partial wave decomposition of the Born kernel is carried out numerically through Eq. (2.26). The spin-flavor-color factors in the quark sector are also shown in the operator form in the isospin space.

### B.1. Quark sector

#### Exchange normalization kernel

$$M_N(\mathbf{q}_f, \mathbf{q}_i) = X_N f(\theta) \quad , \quad (\text{B}\cdot 1)$$

with

$$f(\theta) = (\sqrt{3\pi}b)^3 \exp \left\{ -\frac{b^2}{3}(\mathbf{q}^2 + \mathbf{k}^2) \right\} . \quad (\text{B}\cdot 2)$$

#### Exchange kinetic-energy kernel

$$M^K(\mathbf{q}_f, \mathbf{q}_i) = X_N \left[ \frac{1}{3} \left( 2 + \frac{1}{\lambda} \right) + \frac{1}{6} \left( 1 - \frac{1}{\lambda} \right) Y \right] f_{K_1}(\theta) + X_K \frac{1}{6} \left( 1 - \frac{1}{\lambda} \right) f_{K_2}(\theta), \quad (\text{B}\cdot 3)$$

where  $\lambda = (m_s/m_{ud})$ ,  $Y$  is the hypercharge of the total system, and

$$\left. \begin{array}{l} f_{K_1}(\theta) \\ f_{K_2}(\theta) \end{array} \right\} = \frac{3}{4} x^2 m_{ud} c^2 f(\theta) \left\{ \begin{array}{l} \left[ -1 + \frac{1}{3} b^2 (2\mathbf{q}^2 + \mathbf{k}^2) \right] \\ \frac{1}{4} \left[ 1 + \frac{2}{3} b^2 (\mathbf{q}^2 - \mathbf{k}^2) \right] \end{array} \right\} , \quad (\text{B}\cdot 4)$$

with  $x = (\hbar/m_{ud}cb)$ .

Color-Coulombic term

$$M^{CC}(\mathbf{q}_f, \mathbf{q}_i) = X_N \left[ 2 \left( f_E^{CC}(\theta) - f_S^{CC}(\theta) - f_{S'}^{CC}(\theta) \right) + f_{D_+}^{CC}(\theta) + f_{D_-}^{CC}(\theta) \right] , \quad (\text{B}\cdot 5)$$

where

$$f_T^{CC}(\theta) = \sqrt{\frac{2}{\pi}} \alpha_S x m_{ud} c^2 \frac{4}{3} (\sqrt{3\pi} b)^3 \times \begin{cases} \left(\frac{8}{11}\right)^{\frac{1}{2}} \exp \left\{ -\frac{2}{11} b^2 \left[ \frac{4}{3} (\mathbf{q}^2 + \mathbf{k}^2) - \mathbf{k} \cdot \mathbf{q} \right] \right\} \tilde{h}_0 \left( \frac{1}{\sqrt{11}} b |\mathbf{q} + \mathbf{k}| \right) \\ \left(\frac{1}{2}\right)^{\frac{1}{2}} \exp \left\{ -\frac{1}{3} b^2 \left( \mathbf{q}^2 + \frac{1}{4} \mathbf{k}^2 \right) \right\} \tilde{h}_0 \left( \frac{1}{2} b |\mathbf{k}| \right) \\ \left(\frac{2}{3}\right)^{\frac{1}{2}} \exp \left\{ -\frac{1}{3} b^2 \mathbf{k}^2 \right\} \tilde{h}_0 \left( \frac{1}{\sqrt{3}} b |\mathbf{q}| \right) \end{cases} \quad \text{for } \mathcal{T} = \begin{cases} S \\ D_+ \\ D_- \end{cases} . \quad (\text{B}\cdot 6)$$

The  $E$ -type factor is given by  $f_E^{CC}(\theta) = \sqrt{2/\pi} \alpha_S x m_{ud} c^2 (4/3) f(\theta)$ .

Breit retardation term

$$M^{MC}(\mathbf{q}_f, \mathbf{q}_i) = X_E^{MC} \left( f_E^{MC}(\theta) - \frac{4}{9} f_E^{GC}(\theta) \right) + X_{S'}^{MC} \left( f_{S'}^{MC}(\theta) - \frac{4}{9} f_E^{GC}(\theta) \right) + X_S^{MC} f_S^{MC}(\theta) + X_{D_+}^{MC} f_{D_+}^{MC}(\theta) + X_{D_-}^{MC} f_{D_-}^{MC}(\theta) , \quad (\text{B}\cdot 7)$$

where

$$f_T^{MC}(\theta) = \sqrt{\frac{2}{\pi}} \alpha_S x^3 m_{ud} c^2 \frac{2}{9} (\sqrt{3\pi} b)^3 \times \begin{cases} \exp \left\{ -\frac{1}{3} b^2 (\mathbf{q}^2 + \mathbf{k}^2) \right\} \left[ \frac{5}{2} - (b\mathbf{q})^2 \right] & \text{for } \mathcal{T} = E \\ \left(\frac{8}{11}\right)^{\frac{1}{2}} \exp \left\{ -\frac{2}{11} b^2 \left[ \frac{4}{3} (\mathbf{q}^2 + \mathbf{k}^2) - \mathbf{k} \cdot \mathbf{q} \right] \right\} \\ \times \left[ \tilde{H}_0 \left( \frac{1}{\sqrt{11}} b |\mathbf{q} + \mathbf{k}| \right) - \frac{3}{4} b^2 (\mathbf{k} \cdot \mathbf{q}) \tilde{H}_1 \left( \frac{1}{\sqrt{11}} b |\mathbf{q} + \mathbf{k}| \right) \right. \\ \left. + \frac{3}{22} b^4 (\mathbf{q}^2 + \mathbf{k} \cdot \mathbf{q}) (\mathbf{k}^2 + \mathbf{k} \cdot \mathbf{q}) \tilde{H}_2 \left( \frac{1}{\sqrt{11}} b |\mathbf{q} + \mathbf{k}| \right) \right] & \text{for } \mathcal{T} = S \\ \left(\frac{1}{2}\right)^{\frac{1}{2}} \exp \left\{ -\frac{1}{3} b^2 \left( \mathbf{q}^2 + \frac{1}{4} \mathbf{k}^2 \right) \right\} \left[ -\frac{1}{2} \tilde{H}_0 \left( \frac{1}{2} b |\mathbf{k}| \right) \right. \\ \left. + \frac{3}{4} (b\mathbf{q})^2 \tilde{H}_1 \left( \frac{1}{2} b |\mathbf{k}| \right) - \frac{3}{8} b^4 (\mathbf{k} \cdot \mathbf{q})^2 \tilde{H}_2 \left( \frac{1}{2} b |\mathbf{k}| \right) \right] & \text{for } \mathcal{T} = D_+ \\ \left(\frac{2}{3}\right)^{\frac{1}{2}} \exp \left\{ -\frac{1}{3} b^2 \mathbf{k}^2 \right\} \left[ -2 \tilde{H}_0 \left( \frac{1}{\sqrt{3}} b |\mathbf{q}| \right) + \frac{3}{4} (b\mathbf{k})^2 \tilde{H}_1 \left( \frac{1}{\sqrt{3}} b |\mathbf{q}| \right) \right. \\ \left. - \frac{1}{2} b^4 (\mathbf{k} \cdot \mathbf{q})^2 \tilde{H}_2 \left( \frac{1}{\sqrt{3}} b |\mathbf{q}| \right) \right] & \text{for } \mathcal{T} = D_- \end{cases} . \quad (\text{B}\cdot 8)$$

The functions  $\tilde{H}_n(x)$  with  $n = 0, 1, 2$  are expressed by  $\tilde{h}_n(x)$  through

$$\begin{aligned} \tilde{H}_0(x) &= \tilde{h}_0(x) \\ \tilde{H}_1(x) &= \tilde{h}_0(x) + \frac{1}{3} \tilde{h}_1(x) \\ \tilde{H}_2(x) &= \frac{1}{3} \tilde{h}_1(x) - \frac{1}{5} \tilde{h}_2(x) \end{aligned} . \quad (\text{B}\cdot 9)$$

The function  $f_E^{GC}(\theta)$  is given below.

### Color-Magnetic term

$$M^{GC}(\mathbf{q}_f, \mathbf{q}_i) = -X_{S'}^{GC} f_E^{GC}(\theta) + \sum_{T \neq E} X_T^{GC} f_T^{GC}(\theta) , \quad (\text{B}\cdot 10)$$

where  $f_E^{GC}(\theta) = \sqrt{2/\pi} \alpha_S x^3 m_{ud} c^2 f(\theta)$  and

$$f_T^{GC}(\theta) = \sqrt{\frac{2}{\pi}} \alpha_S x^3 m_{ud} c^2 (\sqrt{3\pi} b)^3 \times \begin{cases} \left(\frac{8}{11}\right)^{\frac{3}{2}} \exp\left\{-\frac{2}{11} b^2 \left[\frac{4}{3}(\mathbf{q}^2 + \mathbf{k}^2) - \mathbf{k} \cdot \mathbf{q}\right]\right\} \\ \left(\frac{1}{2}\right)^{\frac{3}{2}} \exp\left\{-\frac{1}{3} b^2 \left(\mathbf{q}^2 + \frac{1}{4} \mathbf{k}^2\right)\right\} \\ \left(\frac{2}{3}\right)^{\frac{3}{2}} \exp\left\{-\frac{1}{3} b^2 \mathbf{k}^2\right\} \end{cases} \quad \text{for } \mathcal{T} = \begin{cases} S \\ D_+ \\ D_- \end{cases} . \quad (\text{B}\cdot 11)$$

### LS term

In general there are three different types of  $LS$  terms in the  $YN$  interaction; i.e.,  $\Omega = LS, LS^{(-)}$  and  $LS^{(-)\sigma}$ .<sup>17)</sup> These are different only for the spin-flavor-color factors. For each type we have

$$M^\Omega(\mathbf{q}_f, \mathbf{q}_i) = \sum_{T \neq E} X_T^\Omega f_T^{LS}(\theta) , \quad (\text{B}\cdot 12)$$

where

$$f_T^{LS}(\theta) = -\sqrt{\frac{2}{\pi}} \alpha_S x^3 m_{ud} c^2 \frac{1}{2} (3\pi)^{\frac{3}{2}} b^5 \times \begin{cases} \left(\frac{8}{11}\right)^{\frac{3}{2}} \exp\left\{-\frac{2}{11} b^2 \left[\frac{4}{3}(\mathbf{q}^2 + \mathbf{k}^2) - \mathbf{k} \cdot \mathbf{q}\right]\right\} \tilde{h}_1\left(\frac{1}{\sqrt{11}} b |\mathbf{q} + \mathbf{k}|\right) \\ \left(\frac{1}{2}\right)^{\frac{3}{2}} \exp\left\{-\frac{1}{3} b^2 \left(\mathbf{q}^2 + \frac{1}{4} \mathbf{k}^2\right)\right\} \tilde{h}_1\left(\frac{1}{2} b |\mathbf{k}|\right) \\ \left(\frac{2}{3}\right)^{\frac{3}{2}} \exp\left\{-\frac{1}{3} b^2 \mathbf{k}^2\right\} \tilde{h}_1\left(\frac{1}{\sqrt{3}} b |\mathbf{q}|\right) \end{cases} \quad \text{for } \mathcal{T} = \begin{cases} S \\ D_+ \\ D_- \end{cases} . \quad (\text{B}\cdot 13)$$

### Tensor term

There are three different types of tensor terms as in Eq.(2.24).<sup>17)</sup> These are given by

$$\left. \begin{array}{l} M^T(\mathbf{q}_f, \mathbf{q}_i) \\ M^{T'}(\mathbf{q}_f, \mathbf{q}_i) \end{array} \right\} = X_S^T f_S^T(\theta) + X_{S'}^T f_{S'}^T(\theta) + \begin{cases} X_{D_+}^T f_{D_+}^T(\theta) \\ X_{D_-}^T f_{D_-}^T(\theta) \end{cases} , \quad (\text{B}\cdot 14)$$

$$M^{T''}(\mathbf{q}_f, \mathbf{q}_i) = 2 \left[ X_S^T f_S^T(\theta) - X_{S'}^T f_{S'}^T(\theta) \right] , \quad (\text{B}\cdot 14)$$



where

$$f_{\mathcal{T}}^T(\theta) = -\sqrt{\frac{2}{\pi}} \alpha_S x^3 m_{ud} c^2 \frac{2}{5} (3\pi)^{\frac{3}{2}} b^5$$

$$\times \begin{cases} \left(\frac{8}{11}\right)^{\frac{3}{2}} \frac{1}{11} \exp\left\{-\frac{2}{11} b^2 \left[\frac{4}{3}(\mathbf{q}^2 + \mathbf{k}^2) - \mathbf{k} \cdot \mathbf{q}\right]\right\} \tilde{h}_2\left(\frac{1}{\sqrt{11}} b |\mathbf{q} + \mathbf{k}|\right) \\ \left(\frac{1}{2}\right)^{\frac{3}{2}} \frac{1}{4} \exp\left\{-\frac{1}{3} b^2 \left(\mathbf{q}^2 + \frac{1}{4} \mathbf{k}^2\right)\right\} \tilde{h}_2\left(\frac{1}{2} b |\mathbf{k}|\right) \\ \left(\frac{2}{3}\right)^{\frac{3}{2}} \frac{1}{3} \exp\left\{-\frac{1}{3} b^2 \mathbf{k}^2\right\} \tilde{h}_2\left(\frac{1}{\sqrt{3}} b |\mathbf{q}|\right) \end{cases} \quad \text{for } \mathcal{T} = \begin{cases} S \\ D_+ \\ D_- \end{cases} .$$

(B.15)

## B.2. EMEP sector

### Direct terms

The S-meson central (CN), PS-meson spin-spin (SN) and PS-meson tensor (TN) terms are given by

$$\begin{aligned} M_D^{CN}(\mathbf{q}_f, \mathbf{q}_i) &= X_{0D_+}^{CN} f_D^{CN}(\theta) , \\ M_D^{SN}(\mathbf{q}_f, \mathbf{q}_i) &= X_{0D_+}^T (\boldsymbol{\sigma}_1 \cdot \boldsymbol{\sigma}_2) f_D^{SN}(\theta) , \\ M_D^{TN}(\mathbf{q}_f, \mathbf{q}_i) &= X_{0D_+}^T f_D^{TN}(\theta) , \end{aligned} \quad (\text{B.16})$$

where

$$\begin{aligned} f_D^{CN}(\theta) &= -4\pi \hbar c \frac{1}{m^2 + \mathbf{k}^2} e^{-\frac{1}{3}(b\mathbf{k})^2} , \\ f_D^{SN}(\theta) &= 4\pi \hbar c \frac{1}{3} \left( \frac{1}{m^2 + \mathbf{k}^2} - c_\delta \frac{1}{m^2} \right) e^{-\frac{1}{3}(b\mathbf{k})^2} , \\ f_D^{TN}(\theta) &= -4\pi \hbar c \frac{1}{3m^2} \frac{1}{m^2 + \mathbf{k}^2} e^{-\frac{1}{3}(b\mathbf{k})^2} = \frac{1}{3m^2} f_D^{CN}(\theta) . \end{aligned} \quad (\text{B.17})$$

Here  $m$  ( $= mc/\hbar$ ) is the meson mass, and the relationship  $X_{0D_+}^{SN} = X_{0D_+}^T (\boldsymbol{\sigma}_1 \cdot \boldsymbol{\sigma}_2)$  is used in Eq. (B.16). The factor  $c_\delta$  in Eq. (B.17) is a reduction factor for the spin-spin contact term of the PS-mesons.

### Exchange terms

$$\begin{aligned} M_{(SN)}^{(CN)}(\mathbf{q}_f, \mathbf{q}_i) &= -X_{1S'}^{(CN)} f_E^{(CN)}(\theta) + \sum_{\mathcal{T} \neq E} X_{1\mathcal{T}}^{(CN)} f_{\mathcal{T}}^{(CN)}(\theta) , \\ \left. \begin{aligned} M^{TN}(\mathbf{q}_f, \mathbf{q}_i) \\ M^{TN'}(\mathbf{q}_f, \mathbf{q}_i) \end{aligned} \right\} &= X_{1S}^T f_S^{TN}(\theta) + X_{1S'}^T f_{S'}^{TN}(\theta) + \begin{cases} X_{1D_+}^T f_{D_+}^{TN}(\theta) \\ X_{1D_-}^T f_{D_-}^{TN}(\theta) \end{cases} , \\ M^{TN''}(\mathbf{q}_f, \mathbf{q}_i) &= 2 \left[ X_{1S}^T f_S^{TN}(\theta) - X_{1S'}^T f_{S'}^{TN}(\theta) \right] , \end{aligned} \quad (\text{B.18})$$

where

$$\left. \begin{aligned} f_{\mathcal{T}}^{CN}(\theta) \\ f_{\mathcal{T}}^{SN}(\theta) \end{aligned} \right\} = -4\pi \begin{cases} 1 \\ -\frac{1}{3} \end{cases} \left(\frac{3}{2}\right)^{\frac{3}{2}} \hbar c b^2$$

$$\begin{aligned}
& \times \begin{cases} \exp \left\{ -\frac{1}{3}b^2(\mathbf{q}^2 + \mathbf{k}^2) \right\} \left[ \tilde{\mathcal{Y}}_{\alpha_E}(0) - \left\{ \begin{array}{c} 0 \\ c_{\delta} \frac{1}{2\alpha_E} \end{array} \right\} \right] & \text{for } E \\ \left( \frac{8}{11} \right)^{\frac{1}{2}} \exp \left\{ -\frac{2}{11}b^2 \left[ \frac{4}{3}(\mathbf{q}^2 + \mathbf{k}^2) - \mathbf{k} \cdot \mathbf{q} \right] \right\} \left[ \tilde{\mathcal{Y}}_{\alpha_S} \left( \frac{1}{\sqrt{11}}b|\mathbf{q} + \mathbf{k}| \right) - \left\{ \begin{array}{c} 0 \\ c_{\delta} \frac{1}{2\alpha_S} \end{array} \right\} \right] & \text{for } \mathcal{T} = S \\ \left( \frac{1}{2} \right)^{\frac{1}{2}} \exp \left\{ -\frac{1}{3}b^2 \left( \mathbf{q}^2 + \frac{1}{4}\mathbf{k}^2 \right) \right\} \left[ \tilde{\mathcal{Y}}_{\alpha_{D_+}} \left( \frac{1}{2}b|\mathbf{k}| \right) - \left\{ \begin{array}{c} 0 \\ c_{\delta} \frac{1}{2\alpha_{D_+}} \end{array} \right\} \right] & \text{for } \mathcal{T} = D_+ \\ \left( \frac{2}{3} \right)^{\frac{1}{2}} \exp \left\{ -\frac{1}{3}b^2\mathbf{k}^2 \right\} \left[ \tilde{\mathcal{Y}}_{\alpha_{D_-}} \left( \frac{1}{\sqrt{3}}b|\mathbf{q}| \right) - \left\{ \begin{array}{c} 0 \\ c_{\delta} \frac{1}{2\alpha_{D_-}} \end{array} \right\} \right] & \text{for } \mathcal{T} = D_- , \end{cases} \\
f_{\mathcal{T}}^{TN}(\theta) &= -4\pi \left( \frac{3}{2} \right)^{\frac{1}{2}} \hbar cb^2 \left( \frac{\hbar}{mc} \right)^2 \\
& \times \begin{cases} \left( \frac{8}{11} \right)^{\frac{3}{2}} \frac{1}{11} \exp \left\{ -\frac{2}{11}b^2 \left[ \frac{4}{3}(\mathbf{q}^2 + \mathbf{k}^2) - \mathbf{k} \cdot \mathbf{q} \right] \right\} \tilde{\mathcal{Z}}_{\alpha_S} \left( \frac{1}{\sqrt{11}}b|\mathbf{q} + \mathbf{k}| \right) & \text{for } \mathcal{T} = S \\ \left( \frac{1}{2} \right)^{\frac{3}{2}} \frac{1}{4} \exp \left\{ -\frac{1}{3}b^2 \left( \mathbf{q}^2 + \frac{1}{4}\mathbf{k}^2 \right) \right\} \tilde{\mathcal{Z}}_{\alpha_{D_+}} \left( \frac{1}{2}b|\mathbf{k}| \right) & \text{for } \mathcal{T} = D_+ \\ \left( \frac{2}{3} \right)^{\frac{3}{2}} \frac{1}{3} \exp \left\{ -\frac{1}{3}b^2\mathbf{k}^2 \right\} \tilde{\mathcal{Z}}_{\alpha_{D_-}} \left( \frac{1}{\sqrt{3}}b|\mathbf{q}| \right) & \text{for } \mathcal{T} = D_- . \end{cases} \quad (\text{B.19})
\end{aligned}$$

The coefficients  $\alpha_{\mathcal{T}}$  are given by  $\alpha_S = \alpha_{S'} = (11/8)\alpha_E$ ,  $\alpha_{D_+} = 2\alpha_E$ , and  $\alpha_{D_-} = (3/2)\alpha_E$ , with  $\alpha_E = (mb)^2/2 = (1/2)(mcb/\hbar)^2$ .

### B.3. Spin-flavor-color factors in the quark sector

The spin-flavor-color factors in the quark sector for the  $NN$  system are given in Eq.(B.6) of Ref.25). We should note that  $X_{\mathcal{T}}$  there is actually  $X_{\mathcal{T}}^{GC}$  for  $\mathcal{T} = D_+$  and  $D_-$ , and  $X_S^{GC} = X_{S'}^{GC} = -X_E$ . (Note that  $X_E$  is not  $X_E^{GC}$ .) Furthermore,  $X_{D_-}^{MC} = X_{D_+}^{MC} = X_N$ ,  $X_S^{MC} = X_{S'}^{MC} = -2X_N$ ,  $X_E^{MC} = -X^N$ , and  $X_K = 0$  for  $NN$ . The spin-orbit and tensor factors for  $YN$  systems are found in Appendix C of Ref.17). Here we list up the one-quark exchange ( $x = 1$ ) central factors  $(X_{\mathcal{T}}^Q)_{B_3B_1}$  in Eq.(A.3), with respect to the quark sector of the  $\Lambda N$ ,  $\Sigma N$  and  $\Xi N$  systems. The spin-flavor factors in the EMEP sector and the detailed derivation of these factors will be published elsewhere. In the following, the parameter  $\lambda (= m_s/m_{ud}^*)$  controls the flavor symmetry breaking of the FB interaction. The spin and isospin operators,  $\boldsymbol{\sigma}_i$  and  $\boldsymbol{\tau}_i$ , are with respect to the two baryons  $B_i$  with  $i = 1$  or  $2$  in the initial state, and the flavor exchange operator  $P_F$  is supposed to operate on the ket state. We assume  $B_2 = B_4 = N$ . The spin-flavor-color factor for the exchange normalization kernel is given by  $X_N = X_{D_-}^{MC}(\lambda = 1)$ . The factors of the interaction type  $\mathcal{T} = S'$  are discussed in § 5 of Ref.17).

$$[ B_3B_1 = \Lambda\Lambda ]$$

$$\begin{aligned}
X_K &= 1 - (1 + \boldsymbol{\sigma}_1 \cdot \boldsymbol{\sigma}_2)P_F , \\
X_{D_-}^{MC} &= -\frac{1}{4} \left[ 2 + \frac{1}{\lambda} (1 + \boldsymbol{\sigma}_1 \cdot \boldsymbol{\sigma}_2) P_F \right] ,
\end{aligned}$$

---

\*)  $\lambda = m_{ud}/m_s$  in Ref.17) is a misprint.

$$\begin{aligned}
X_{D_+}^{MC} &= -\frac{1}{4} \left[ 1 + \frac{1}{\lambda} + (1 + \boldsymbol{\sigma}_1 \cdot \boldsymbol{\sigma}_2) P_F \right] , \\
X_S^{MC} &= \frac{1}{4} \left[ 3 + \frac{1}{\lambda} + \left( 1 + \frac{1}{\lambda} \right) (1 + \boldsymbol{\sigma}_1 \cdot \boldsymbol{\sigma}_2) P_F \right] , \\
X_{D_-}^{GC} &= \frac{1}{2} + \frac{1}{24} \left[ \left( 1 + \frac{4}{\lambda} + \frac{1}{\lambda^2} \right) + (\boldsymbol{\sigma}_1 \cdot \boldsymbol{\sigma}_2) \left( 1 - \frac{4}{3\lambda} + \frac{1}{\lambda^2} \right) \right] P_F , \\
X_{D_+}^{GC} &= \frac{1}{72} \left[ \left( 13 + \frac{3}{\lambda^2} \right) + 6P_F + (\boldsymbol{\sigma}_1 \cdot \boldsymbol{\sigma}_2) \left( \frac{4}{3\lambda} + 6P_F \right) \right] , \\
X_S^{GC} &= -\frac{1}{72} \left\{ \left( 1 + \frac{3}{\lambda^2} \right) + 3 \left( 3 + \frac{1}{\lambda^2} \right) P_F + (\boldsymbol{\sigma}_1 \cdot \boldsymbol{\sigma}_2) \left[ \frac{4}{3\lambda} + 3 \left( 3 + \frac{1}{\lambda^2} \right) P_F \right] \right\} .
\end{aligned} \tag{B.20}$$

$$[ B_3 B_1 = \Sigma \Sigma ]$$

$$\begin{aligned}
X_K &= 1 + \frac{1}{3} \boldsymbol{\tau}_1 \cdot \boldsymbol{\tau}_2 - \frac{1}{3} (1 + \boldsymbol{\tau}_1 \cdot \boldsymbol{\tau}_2) P_F + (\boldsymbol{\sigma}_1 \cdot \boldsymbol{\sigma}_2) \frac{2}{9} \left[ 1 + \frac{5}{3} \boldsymbol{\tau}_1 \cdot \boldsymbol{\tau}_2 - \frac{1}{6} (1 + \boldsymbol{\tau}_1 \cdot \boldsymbol{\tau}_2) P_F \right] , \\
X_{D_-}^{MC} &= -\frac{1}{2} \left\{ 1 + \frac{1}{3} \boldsymbol{\tau}_1 \cdot \boldsymbol{\tau}_2 + \frac{1}{6\lambda} (1 + \boldsymbol{\tau}_1 \cdot \boldsymbol{\tau}_2) P_F \right. \\
&\quad \left. + (\boldsymbol{\sigma}_1 \cdot \boldsymbol{\sigma}_2) \frac{2}{9} \left[ 1 + \frac{5}{3} \boldsymbol{\tau}_1 \cdot \boldsymbol{\tau}_2 + \frac{1}{12\lambda} (1 + \boldsymbol{\tau}_1 \cdot \boldsymbol{\tau}_2) P_F \right] \right\} , \\
X_{D_+}^{MC} &= -\frac{1}{4} \left( 1 + \frac{1}{\lambda} \right) \left[ 1 + \frac{1}{3} \boldsymbol{\tau}_1 \cdot \boldsymbol{\tau}_2 + (\boldsymbol{\sigma}_1 \cdot \boldsymbol{\sigma}_2) \frac{2}{9} \left( 1 + \frac{5}{3} \boldsymbol{\tau}_1 \cdot \boldsymbol{\tau}_2 \right) \right] \\
&\quad - \frac{1}{12} \left( 1 + \frac{1}{9} \boldsymbol{\sigma}_1 \cdot \boldsymbol{\sigma}_2 \right) (1 + \boldsymbol{\tau}_1 \cdot \boldsymbol{\tau}_2) P_F , \\
X_S^{MC} &= \frac{1}{4} \left( 3 + \frac{1}{\lambda} \right) \left[ 1 + \frac{1}{3} \boldsymbol{\tau}_1 \cdot \boldsymbol{\tau}_2 + (\boldsymbol{\sigma}_1 \cdot \boldsymbol{\sigma}_2) \frac{2}{9} \left( 1 + \frac{5}{3} \boldsymbol{\tau}_1 \cdot \boldsymbol{\tau}_2 \right) \right] \\
&\quad + \frac{1}{12} \left( 1 + \frac{1}{\lambda} \right) \left( 1 + \frac{1}{9} \boldsymbol{\sigma}_1 \cdot \boldsymbol{\sigma}_2 \right) (1 + \boldsymbol{\tau}_1 \cdot \boldsymbol{\tau}_2) P_F , \\
X_{D_-}^{GC} &= \frac{1}{2} \left( 1 + \frac{1}{3} \boldsymbol{\tau}_1 \cdot \boldsymbol{\tau}_2 \right) + \frac{1}{72} \left( 1 + \frac{4}{\lambda} + \frac{1}{\lambda^2} \right) (1 + \boldsymbol{\tau}_1 \cdot \boldsymbol{\tau}_2) P_F \\
&\quad + (\boldsymbol{\sigma}_1 \cdot \boldsymbol{\sigma}_2) \frac{1}{81} \left[ 1 + \frac{5}{3} \boldsymbol{\tau}_1 \cdot \boldsymbol{\tau}_2 + \frac{1}{8} \left( 1 - \frac{4}{3\lambda} + \frac{1}{\lambda^2} \right) (1 + \boldsymbol{\tau}_1 \cdot \boldsymbol{\tau}_2) P_F \right] , \\
X_{D_+}^{GC} &= \frac{1}{3 \cdot 72} \left\{ \left( 23 + \frac{8}{\lambda} + \frac{9}{\lambda^2} \right) + \frac{1}{3} \left( 31 - \frac{8}{\lambda} + \frac{9}{\lambda^2} \right) \boldsymbol{\tau}_1 \cdot \boldsymbol{\tau}_2 + \frac{34}{3} (1 + \boldsymbol{\tau}_1 \cdot \boldsymbol{\tau}_2) P_F \right. \\
&\quad \left. + (\boldsymbol{\sigma}_1 \cdot \boldsymbol{\sigma}_2) \frac{2}{3} \left[ \left( 13 - \frac{2}{\lambda} + \frac{3}{\lambda^2} \right) + \frac{1}{3} \left( 41 + \frac{2}{\lambda} + \frac{15}{\lambda^2} \right) \boldsymbol{\tau}_1 \cdot \boldsymbol{\tau}_2 + \frac{11}{3} (1 + \boldsymbol{\tau}_1 \cdot \boldsymbol{\tau}_2) P_F \right] \right\} , \\
X_S^{GC} &= -\frac{1}{72} \left\{ \left( 17 - \frac{8}{\lambda} + \frac{3}{\lambda^2} \right) + \left( 11 - \frac{8}{3\lambda} + \frac{1}{\lambda^2} \right) \boldsymbol{\tau}_1 \cdot \boldsymbol{\tau}_2 \right. \\
&\quad + \frac{1}{3} \left( 1 - \frac{8}{\lambda} + \frac{3}{\lambda^2} \right) (1 + \boldsymbol{\tau}_1 \cdot \boldsymbol{\tau}_2) P_F + (\boldsymbol{\sigma}_1 \cdot \boldsymbol{\sigma}_2) \frac{1}{9} \left[ 6 \left( 11 - \frac{2}{3\lambda} + \frac{1}{\lambda^2} \right) \right. \\
&\quad \left. \left. + 2 \left( 39 - \frac{10}{3\lambda} + \frac{5}{\lambda^2} \right) \boldsymbol{\tau}_1 \cdot \boldsymbol{\tau}_2 + \frac{1}{3} \left( 1 - \frac{8}{\lambda} + \frac{3}{\lambda^2} \right) (1 + \boldsymbol{\tau}_1 \cdot \boldsymbol{\tau}_2) P_F \right] \right\} . \tag{B.21}
\end{aligned}$$

[  $B_3 B_1 = \Xi \Xi$  ]

$$\begin{aligned}
X_K &= 1 + \frac{1}{3} \boldsymbol{\tau}_1 \cdot \boldsymbol{\tau}_2 - (\boldsymbol{\sigma}_1 \cdot \boldsymbol{\sigma}_2) \frac{1}{9} \left( 1 + \frac{5}{3} \boldsymbol{\tau}_1 \cdot \boldsymbol{\tau}_2 \right) , & X_N &= -\frac{1}{4} X_K , \\
X_{D_-}^{MC} &= X_N , & X_{D_+}^{MC} &= \frac{1}{\lambda} X_N , & X_S^{MC} &= -\left( 1 + \frac{1}{\lambda} \right) X_N , \\
X_{D_-}^{GC} &= \frac{1}{4} \left[ 1 + \frac{1}{3} \boldsymbol{\tau}_1 \cdot \boldsymbol{\tau}_2 - (\boldsymbol{\sigma}_1 \cdot \boldsymbol{\sigma}_2) \frac{1}{81} \left( 1 + \frac{5}{3} \boldsymbol{\tau}_1 \cdot \boldsymbol{\tau}_2 \right) \right] , \\
X_{D_+}^{GC} &= \frac{1}{3 \cdot 72} \left\{ \left( 9 + \frac{8}{\lambda} + \frac{9}{\lambda^2} \right) + \frac{1}{3} \left( 9 - \frac{8}{\lambda} + \frac{9}{\lambda^2} \right) \boldsymbol{\tau}_1 \cdot \boldsymbol{\tau}_2 \right. \\
&\quad \left. - (\boldsymbol{\sigma}_1 \cdot \boldsymbol{\sigma}_2) \frac{1}{3} \left[ \left( 3 - \frac{8}{\lambda} + \frac{3}{\lambda^2} \right) + \frac{1}{3} \left( 15 + \frac{8}{\lambda} + \frac{15}{\lambda^2} \right) \boldsymbol{\tau}_1 \cdot \boldsymbol{\tau}_2 \right] \right\} , \\
X_S^{GC} &= -\frac{1}{72} \left\{ \left( 5 - \frac{8}{\lambda} + \frac{3}{\lambda^2} \right) + \frac{1}{3} \left( 13 - \frac{8}{\lambda} + \frac{3}{\lambda^2} \right) \boldsymbol{\tau}_1 \cdot \boldsymbol{\tau}_2 \right. \\
&\quad \left. - (\boldsymbol{\sigma}_1 \cdot \boldsymbol{\sigma}_2) \frac{1}{9} \left[ \left( 13 - \frac{8}{\lambda} + \frac{3}{\lambda^2} \right) + \frac{1}{3} \left( 41 - \frac{40}{\lambda} + \frac{15}{\lambda^2} \right) \boldsymbol{\tau}_1 \cdot \boldsymbol{\tau}_2 \right] \right\} . \quad (\text{B}\cdot\text{22})
\end{aligned}$$

[  $B_3 B_1 = \Lambda \Sigma$  and  $\Sigma \Lambda$  ]

$$\begin{aligned}
X_K &= P_F - (\boldsymbol{\sigma}_1 \cdot \boldsymbol{\sigma}_2) \frac{1}{3} \left( \frac{5}{3} + P_F \right) , \\
X_{D_-}^{MC} &= \frac{1}{4} \left[ \frac{1}{\lambda} P_F + (\boldsymbol{\sigma}_1 \cdot \boldsymbol{\sigma}_2) \frac{1}{3} \left( \frac{10}{3} - \frac{1}{\lambda} P_F \right) \right] , \\
X_{D_+}^{MC} &= \frac{5}{36} \left( 1 + \frac{1}{\lambda} \right) (\boldsymbol{\sigma}_1 \cdot \boldsymbol{\sigma}_2) + \frac{1}{4} \left( 1 - \frac{1}{3} \boldsymbol{\sigma}_1 \cdot \boldsymbol{\sigma}_2 \right) P_F , \\
X_S^{MC} &= -\frac{5}{36} \left( 3 + \frac{1}{\lambda} \right) (\boldsymbol{\sigma}_1 \cdot \boldsymbol{\sigma}_2) - \frac{1}{4} \left( 1 + \frac{1}{\lambda} \right) \left( 1 - \frac{1}{3} \boldsymbol{\sigma}_1 \cdot \boldsymbol{\sigma}_2 \right) P_F , \\
X_{D_-}^{GC} &= -\frac{5}{2 \cdot 81} (\boldsymbol{\sigma}_1 \cdot \boldsymbol{\sigma}_2) - \frac{1}{24} \left[ \left( 1 + \frac{4}{\lambda} + \frac{1}{\lambda^2} \right) - (\boldsymbol{\sigma}_1 \cdot \boldsymbol{\sigma}_2) \frac{1}{3} \left( 1 - \frac{4}{3\lambda} + \frac{1}{\lambda^2} \right) \right] P_F , \\
X_{D_+}^{GC} &= -\frac{1}{3 \cdot 36} \left[ \left( \frac{2}{\lambda} + 9P_F \right) + (\boldsymbol{\sigma}_1 \cdot \boldsymbol{\sigma}_2) \frac{1}{6} \left( 49 + \frac{15}{\lambda^2} - 18P_F \right) \right] , \\
X_S^{GC} &= \begin{cases} \frac{1}{72} \left\{ \frac{4}{\lambda} + \left( 9 - \frac{8}{\lambda} + \frac{3}{\lambda^2} \right) P_F \right. \\ \quad \left. + (\boldsymbol{\sigma}_1 \cdot \boldsymbol{\sigma}_2) \frac{1}{3} \left[ \left( 39 - \frac{40}{3\lambda} + \frac{5}{\lambda^2} \right) - \left( 9 - \frac{8}{\lambda} + \frac{3}{\lambda^2} \right) P_F \right] \right\} \\ \frac{1}{72} \left\{ \frac{4}{\lambda} + \left( 1 + \frac{3}{\lambda^2} \right) P_F \right. \\ \quad \left. + (\boldsymbol{\sigma}_1 \cdot \boldsymbol{\sigma}_2) \frac{1}{3} \left[ \left( \frac{37}{3} + \frac{40}{3\lambda} + \frac{5}{\lambda^2} \right) - \left( 1 + \frac{3}{\lambda^2} \right) P_F \right] \right\} \end{cases} \\
&\quad \text{for } \begin{cases} \Lambda \Sigma \\ \Sigma \Lambda \end{cases} . \quad (\text{B}\cdot\text{23})
\end{aligned}$$

### Appendix C

— Partial-wave decomposition of the Born kernel —

In this appendix we derive some formulae for the partial-wave decomposition of the Born kernel. Suppose the basic Born kernel Eq. (2·22) is expanded into partial waves as

$$\begin{aligned} M(\mathbf{q}_f, \mathbf{q}_i) &= \sum_{\Omega} M^{\Omega}(\mathbf{q}_f, \mathbf{q}_i) \mathcal{O}^{\Omega}(\mathbf{q}_f, \mathbf{q}_i) \\ &= \sum_{JM\ell\ell'S'} 4\pi R_{S'\ell',S\ell}^J(q_f, q_i) \mathcal{Y}_{(\ell'S')JM}(\hat{\mathbf{q}}_f; spin) \mathcal{Y}_{(\ell S)JM}^*(\hat{\mathbf{q}}_i; spin) \quad , \quad (\text{C}\cdot\text{1}) \end{aligned}$$

where  $\mathcal{Y}_{(\ell S)JM}(\hat{\mathbf{q}}; spin) = [Y_{\ell}(\tilde{\mathbf{q}})\chi_S(spin)]_{JM}$  is the standard space-spin function. We can show that the partial-wave components are given by

$$\begin{aligned} R_{S'\ell',S\ell}^J(q_f, q_i) &= \sum_{\Omega} R_{S'\ell',S\ell}^{\Omega J}(q_f, q_i) \quad , \\ R_{S'\ell',S\ell}^{\Omega J}(q_f, q_i) &= \frac{1}{2} \int_{-1}^1 M^{\Omega}(\mathbf{q}_f, \mathbf{q}_i) I_{S'\ell',S\ell}^{\Omega J}(\theta) d(\cos \theta) \quad , \quad (\text{C}\cdot\text{2}) \end{aligned}$$

with  $\cos \theta = (\hat{\mathbf{q}}_f \cdot \hat{\mathbf{q}}_i)$  and

$$I_{S'\ell',S\ell}^{\Omega J}(\theta) = \frac{4\pi}{2J+1} \sum_M \langle \mathcal{Y}_{(\ell'S')JM}(\hat{\mathbf{q}}_f; spin) | \mathcal{O}^{\Omega}(\mathbf{q}_f, \mathbf{q}_i) | \mathcal{Y}_{(\ell S)JM}(\hat{\mathbf{q}}_i; spin) \rangle_{spin} \quad , \quad (\text{C}\cdot\text{3})$$

by using the rotational invariance of  $R_{S'\ell',S\ell}^{\Omega J}(q_f, q_i)$ . In Eq. (C·3) the matrix elements are with respect to the spin variables. For the spin-independent central ( $\mathcal{O}^{CC} = 1$ ) and the spin-spin ( $\mathcal{O}^{SS} = (\boldsymbol{\sigma}_1 \cdot \boldsymbol{\sigma}_2)$ ) terms, the factors Eq. (C·3) are given by

$$I_{S'\ell',S\ell}^{\{CC\}^J}(\theta) = \delta_{S',S} \delta_{\ell',\ell} \left\{ \begin{matrix} 1 \\ [2S(S+1) - 3] \end{matrix} \right\} P_{\ell}(\cos \theta) \quad . \quad (\text{C}\cdot\text{4})$$

For the  $LS$  and tensor terms with Eqs. (2·23) and (2·24), some calculations using the angular-momentum algebra yield

$$\begin{aligned} I_{S'\ell',S\ell}^{LS,J}(\theta) &= -\delta_{S,1} \delta_{S',S} \delta_{\ell',\ell} q_f q_i \frac{1}{2} \left[ 1 + \frac{2 - J(J+1)}{\ell(\ell+1)} \right] \\ &\quad \times \sin \theta P_{\ell}^1(\cos \theta) \quad \text{for } \ell = J, J \pm 1 \quad , \\ I_{S'\ell',S\ell}^{\left\{ \begin{matrix} LS^{(-)} \\ LS^{(-)\sigma} \end{matrix} \right\}^J}(\theta) &= \delta_{J,\ell} \delta_{\ell',\ell} \left\{ \begin{matrix} 1 \\ [S(S+1) - 1] \end{matrix} \right\} q_f q_i \frac{1}{\sqrt{J(J+1)}} \sin \theta P_J^1(\cos \theta) \\ &\quad \text{for } S', S = 0, 1 \text{ or } 1, 0 \quad , \\ I_{1\ell',1\ell}^{\left\{ \begin{matrix} T \\ T' \end{matrix} \right\}^J}(\theta) &= \left\{ \begin{matrix} 1 \\ \frac{1}{4} \end{matrix} \right\} (S_{12})_{\ell',\ell}^J \left[ q_f^2 P_{\ell}(\cos \theta) + q_i^2 P_{\ell'}(\cos \theta) \right. \\ &\quad \left. \mp 2q_f q_i \left\{ \begin{matrix} P_J(\cos \theta) \\ \cos \theta P_{\ell}(\cos \theta) + \frac{3}{2} \frac{1}{\ell(\ell+1)} \sin \theta P_{\ell}^1(\cos \theta) \end{matrix} \right\} \right] \end{aligned}$$

$$\text{for } \begin{cases} \ell' = \ell \pm 2 & \text{and } J = \ell \pm 1 \\ \ell = \ell' = J, & J \pm 1 \end{cases} ,$$

$$I_{1\ell',1\ell}^{T''J}(\theta) = \frac{1}{2}(S_{12})_{\ell',\ell}^J \left[ q_f^2 P_\ell(\cos\theta) - q_i^2 P_{\ell'}(\cos\theta) \right] . \quad (\text{C}\cdot 5)$$

Here  $P_J^1(\cos\theta) = \sin\theta P_J'(\cos\theta)$  is the associated Legendre function of the first kind with degree 1, and  $(S_{12})_{\ell',\ell}^J$  is the standard tensor matrix elements. The final braces in  $I_{1\ell',1\ell}^{\{T/T'\}J}(\theta)$  in Eq. (C·5) are applied to the choice of  $\ell$  and  $\ell'$ . Note that the  $LS$  and tensor components are non-zero only for the spin triplet states, while the  $LS^{(-)}$  and  $LS^{(-)\sigma}$  components are accompanied with the spin transition between  $S = 0$  and 1.

The partial-wave components of the full Born kernel,  $V_{S'\ell',S\ell}^J(q_f, q_i)$  in Eqs. (2·27) and (2·28), are easily obtained from the above formulae.

## Appendix D

### — Partial-wave decomposition of invariant amplitudes —

Reconstruction of the invariant amplitudes in terms of the  $S$ -matrices is an opposite process to the partial-wave decomposition of the Born amplitudes, given in the preceding appendix. We can use the same formulae, Eqs. (C·4) and (C·5), to derive the following result for the partial-wave decomposition of the invariant amplitudes.

Suppose the invariant amplitudes Eq. (2·29) in the isospin basis has the following decomposition:

$$\begin{aligned} M_{ca}(\mathbf{q}_f, \mathbf{q}_i) &= \sqrt{(1 + \delta_{c_1, c_2})(1 + \delta_{a_1, a_2})} \\ &\times \sum_{JM\ell\ell'SS'} 4\pi R_{\gamma S'\ell', \alpha S\ell}^J \mathcal{Y}_{(\ell'S')JM}(\hat{\mathbf{q}}_f; \text{spin}) \mathcal{Y}_{(\ell S)JM}^*(\hat{\mathbf{q}}_i; \text{spin}) . \quad (\text{D}\cdot 1) \end{aligned}$$

Here  $a = (a_1, a_2)$  and  $c = (c_1, c_2)$  imply two-baryon configurations corresponding to the initial and final states,  $\alpha$  and  $\gamma$ , respectively. The front factor,  $\sqrt{(1 + \delta_{c_1, c_2})} \times \sqrt{(1 + \delta_{a_1, a_2})}$ , is a factor for two identical particles, and is 2 for  $NN$ , for example. Without this trivial factor, the invariant amplitudes for a fixed  $ca$  are given by

$$\begin{aligned} \left. \begin{aligned} g_0 \\ g_{ss} \end{aligned} \right\} &= \frac{1}{4} \sum_{J\ell S} (2J+1) \left\{ \begin{array}{c} 1 \\ \frac{1}{3}[2S(S+1) - 3] \end{array} \right\} R_{S\ell, S\ell}^J P_\ell(\cos\theta) , \\ h_0 &= -\frac{1}{4} \sum_J \frac{(2J+1)}{J(J+1)} \left[ R_{1J, 1J}^J P_J^1(\cos\theta) \right. \\ &\quad \left. + J R_{1J+1, 1J+1}^J P_{J+1}^1(\cos\theta) - (J+1) R_{1J-1, 1J-1}^J P_{J-1}^1(\cos\theta) \right] , \\ h_- &= \frac{1}{4} \sum_J \frac{(2J+1)}{\sqrt{J(J+1)}} \left[ R_{1J, 0J}^J + R_{0J, 1J}^J \right] P_J^1(\cos\theta) , \\ f_- &= -\frac{1}{4} \sum_J \frac{(2J+1)}{\sqrt{J(J+1)}} \left[ R_{1J, 0J}^J - R_{0J, 1J}^J \right] P_J^1(\cos\theta) , \end{aligned}$$

$$\begin{aligned}
h_{\left(\begin{smallmatrix} k \\ \mathcal{P} \end{smallmatrix}\right)} &= g_{ss} + h^{(0)} - \frac{\cos \theta}{\sin \theta} h^{(1)} + \frac{1}{\sin \theta} h^{(3)} \\
&\mp \left\{ \cos(\theta - 2\phi) \left[ h^{(2)} - \frac{\cos \theta}{\sin \theta} h^{(3)} + \frac{1}{\sin \theta} h^{(1)} \right] - \sin(\theta - 2\phi) f^{(1)} \right\} , \\
h_n &= g_{ss} - 2 \left[ h^{(0)} - \frac{\cos \theta}{\sin \theta} h^{(1)} + \frac{1}{\sin \theta} h^{(3)} \right] , \\
f_+ &= \sin(\theta - 2\phi) \left[ h^{(2)} - \frac{\cos \theta}{\sin \theta} h^{(3)} + \frac{1}{\sin \theta} h^{(1)} \right] + \cos(\theta - 2\phi) f^{(1)} , \quad (\text{D}\cdot 2)
\end{aligned}$$

with

$$\begin{aligned}
h^{(0)} &= \frac{1}{6} \sum_J \left[ (2J+1) R_{1J,1J}^J P_J(\cos \theta) - (J+2) R_{1J+1,1J+1}^J P_{J+1}(\cos \theta) \right. \\
&\quad \left. - (J-1) R_{1J-1,1J-1}^J P_{J-1}(\cos \theta) \right] , \\
h^{(1)} &= \frac{1}{4} \sum_J \left[ \frac{(2J+1)}{J(J+1)} R_{1J,1J}^J P_J^1(\cos \theta) - \frac{1}{(J+1)} R_{1J+1,1J+1}^J P_{J+1}^1(\cos \theta) \right. \\
&\quad \left. - \frac{1}{J} R_{1J-1,1J-1}^J P_{J-1}^1(\cos \theta) \right] , \\
h^{(2)} &= \frac{1}{2} \sum_J \sqrt{J(J+1)} \left[ R_{1J+1,1J-1}^J + R_{1J-1,1J+1}^J \right] P_J(\cos \theta) , \\
h^{(3)} &= \frac{1}{4} \sum_J \frac{1}{\sqrt{J(J+1)}} \left[ R_{1J+1,1J-1}^J + R_{1J-1,1J+1}^J \right] P_J^1(\cos \theta) , \\
f^{(1)} &= \frac{1}{4} \sum_J \frac{(2J+1)}{\sqrt{J(J+1)}} \left[ R_{1J+1,1J-1}^J - R_{1J-1,1J+1}^J \right] P_J^1(\cos \theta) . \quad (\text{D}\cdot 3)
\end{aligned}$$

In Eqs. (D·2) and (D·3) we have used shorthand notation  $R_{S'\ell, S\ell}^J$  to denote  $R_{\gamma S'\ell, \alpha S\ell}^J$ , where the spin values  $S'$  and  $S$  are uniquely specified from  $\gamma$  and  $\alpha$ , respectively. In Eq. (D·1) the summation over  $\mathcal{P}'$  and  $\mathcal{P}$  is already taken by adding up over all possible values of  $\ell$  and  $S$ , for which  $\mathcal{P}$  is uniquely determined through the generalized Pauli principle,  $(-1)^\ell (-1)^{1-S} \mathcal{P} = -1$ . Note that a simple relationship,  $h_k + h_P + h_n = 3g_{ss}$ , holds. The on-shell scattering amplitudes are conveniently expressed by only two angles  $\theta$  and  $\phi$ , the latter of which is defined through  $\cos \phi = \hat{\mathbf{P}} \cdot \hat{\mathbf{q}}_i$  with

$$\cot \phi = \frac{\sin \theta}{|\mathbf{q}_i|/|\mathbf{q}_f| - \cos \theta} . \quad (\text{D}\cdot 4)$$

For the elastic scattering with  $a_1 = c_1$  and  $a_2 = c_2$ , the magnitude of the c.m. momentum is equal before and after the scattering ( $|\mathbf{q}_i| = |\mathbf{q}_f|$ ), thus yielding  $\phi = \theta/2$ . In this case, the time-reversal invariance gives a further simplification for non-zero invariant amplitudes. Since the  $S$ -matrix is symmetric,  $f_-$  in Eq. (D·2) and  $f^{(1)}$  in Eq. (D·3) are both zero. Combining these two conditions, we find that  $f_- = f_+ = 0$  for the elastic scattering. This is the well-known result of six independent invariant amplitudes for the elastic scattering with the time-reversal invariance.

## References

- [1] F. E. Close, *An Introduction to Quarks and Partons* (Academic, London, 1979).
- [2] M. Oka and K. Yazaki, in *Quarks and Nuclei*, ed. W. Weise (World Scientific, Singapore, 1984), p.489; K. Shimizu, Rep. Prog. Phys. **52** (1989), 1; C. W. Wong, Phys. Rep. **136** (1986), 1.
- [3] C. Nakamoto, Y. Suzuki and Y. Fujiwara, Prog. Theor. Phys. **94** (1995), 65.
- [4] Y. Fujiwara, C. Nakamoto and Y. Suzuki, Prog. Theor. Phys. **94** (1995) 215, 353.
- [5] Y. Fujiwara, C. Nakamoto and Y. Suzuki, Phys. Rev. Lett. **76** (1996), 2242.
- [6] Y. Fujiwara, C. Nakamoto and Y. Suzuki, Phys. Rev. **C54** (1996), 2180.
- [7] T. Fujita, Y. Fujiwara, C. Nakamoto and Y. Suzuki, Prog. Theor. Phys. **100** (1998), 931.
- [8] Y. W. Yu, Z. Y. Zhang, P. N. Shen and L. R. Dai, Phys. Rev. **C52** (1995), 3393.
- [9] Z. Y. Zhang, Y. W. Yu, P. N. Shen, L. R. Dai, Amand Faessler and U. Straub, Nucl. Phys. **A625** (1997), 59.
- [10] S. Yang, P. N. Shen, Z. Y. Zhang and Y. W. Yu, Nucl. Phys. **A635** (1998), 146.
- [11] M. Kamimura, Prog. Theor. Phys. Suppl. No. 62 (1977) 236.
- [12] K. Kume and S. Yamaguchi, Phys. Rev. **C48** (1993), 2097.
- [13] H. P. Noyes, Phys. Rev. Lett. **15** (1965), 538.
- [14] K.L. Kowalski, Phys. Rev. Lett. **15** (1965), 798. [Erratum **15** (1965), 908.]
- [15] M. Kohno, Y. Fujiwara, T. Fujita, C. Nakamoto and Y. Suzuki, submitted to Nucl. Phys. A (1999).
- [16] Y. Suzuki, Nucl. Phys. **A430** (1984), 539.
- [17] Y. Fujiwara, C. Nakamoto, Y. Suzuki and Zhang Zong-ye, Prog. Theor. Phys. **97** (1997), 587.
- [18] M. I. Haftel and F. Tabakin, Nucl. Phys. **A158** (1970),1.
- [19] J. M. Blatt, and L. C. Biedenharn, Rev. Mod. Phys. **24** (1952), 258.
- [20] G. E. Brown and A. D. Jackson, *The Nucleon-Nucleon Interaction* (North Holland, Amsterdam, 1976).
- [21] K. Ikeda, R. Tamagaki, S. Saito, H. Horiuchi, A. Tohsaki-Suzuki and M. Kamimura, Prog. Theor. Phys. Suppl. No. 62 (1977), 1.
- [22] Y. Suzuki, Nucl. Phys. **A405** (1983), 40.
- [23] Y. Fujiwara and Y. C. Tang, Memoirs of the Faculty of Science, Kyoto University, Series A of Physics, Astrophysics, Geophysics and Chemistry, Vol. XXXIX, No. 1, Article 5 (1994), 91.
- [24] Y. Fujiwara and K. T. Hecht, Nucl. Phys. **A456** (1986), 669.
- [25] Y. Fujiwara and K. T. Hecht, Nucl. Phys. **A462** (1987), 621.
- [26] Y. Fujiwara, Prog. Theor. Phys. Suppl. No. 91 (1987), 160.
- [27] Y. Fujiwara, Prog. Theor. Phys. **88** (1992), 933.
- [28] H.-J. Schulze, M. Baldo, U. Lombardo, J. Cugnon and A. Lejeune, Phys. Rev. **C57** (1998), 704.
- [29] R. A. Arndt, Scattering Analysis Interactive Dial-up (SAID), Virginia Polytechnic Institute, Blacksburg, Virginia (private communication).
- [30] M. Lacombe, B. Loiseau, J. M. Richard, R. Vinh Mau, J. Côté, P. Pirès and R. de Tournell, Phys. Rev. **C21** (1980), 861.
- [31] R. A. Arndt, L. D. Roper, R. A. Bryan, R. B. Clark, B. J. VerWest and P. Signell, Phys. Rev. **D28** (1983), 97.
- [32] R. A. Bryan and B. L. Scott, Phys. Rev. **164** (1967), 1215.
- [33] P. M. M. Maessen, Th. A. Rijken and J. J. de Swart, Phys. Rev. **C40** (1989), 2226.
- [34] Th. A. Rijken, V. G. J. Stoks and Y. Yamamoto, Phys. Rev. **C59** (1999), 21.
- [35] Y. Fujiwara, M. Kohno, T. Fujita, C. Nakamoto and Y. Suzuki, submitted to Nucl. Phys. A (1999).